R. & M. No. 3542

R. & M. No. 3542

MINISTRY OF TECHNOLOGY

AERONAUTICAL RESEARCH COUNCIL
REPORTS AND MEMORANDA

The Calculation of Turbulent Boundary Layers with Injection

By J. McQuaid

LONDON: HER MAJESTY'S STATIONERY OFFICE
1968
PRICE £1 1*s.* 6*d.* NET

The Calculation of Turbulent Boundary Layers with Injection

By J. McQuaid

Reports and Memoranda No. 3542*
January, 1967

Summary.

A new two-parameter family of mean velocity profiles for turbulent boundary layers with injection is described. The profile model adopted uses the inner law of Stevenson[21], shown elsewhere (McQuaid[15]) to be in good agreement with the constant-pressure measurements of the present author, and the intermittency hypothesis of Sarnecki[19] shown here to be in good agreement with these same measurements. The family is thus analogous to that presented by Thompson[28] for solid-surface boundary layers. Comparisons are made between the family and velocity profiles obtained in layers with pressure gradients of different sign and severity and good agreement is obtained provided the pressure gradient is within limits determined by the reliability of the constant-pressure inner law used in the model. The skin-friction law obtained from the family in terms of the parameters H, R_θ and v_0/U_1 is presented in chart form. The auxiliary equation of Head[7] is shown to give satisfactory predictions of shape-factor development for layers both with and without pressure gradient. A discussion is included on a boundary layer with a discontinuity in the injection velocity distribution, the injection velocity being suddenly reduced to very nearly zero; the region of adjustment to solid-surface conditions downstream of this change is described.

LIST OF CONTENTS

*Replaces A.R.C. 28 668.

LIST OF CONTENTS—*continued*

---

1. *Introduction.*

In a previous paper (McQuaid[14]), an extensive experimental investigation of the incompressible turbulent boundary layer with distributed injection was described. The primary object of that investigation was to obtain data which would allow the extension of an existing solid surface-method to, or the development of a new method for, the calculation of the boundary layer with injection and arbitrary pressure gradient. This calculation requires, as for the equivalent solid-surface calculation, an auxiliary equation for the shape factor, H, and a skin-friction law, to be used with the momentum-integral equation. In this Report, the provision of these two relations, using the new measurements, will be considered.

The skin-friction relation can be obtained if the law governing the whole velocity profile is known. It is now generally recognised that such a law must contain at least two independent parameters if it is adequately to represent velocity profiles in non-equilibrium conditions. This is because the two regions into which the layer is divided each differ in their behaviour in these conditions. The wall region of the layer is characterised by a rapid response to disturbances in local conditions; any such disturbance is rapidly damped out and the velocity profile quickly settles to a state which is independent of the upstream conditions. The outer part, however, responds comparatively slowly to such changes and the outer velocity profile does depend on the upstream history.

This division of the layer has been used as the basis for several methods of representing the overall profile. It has been found for the inner region on solid surfaces that the law of the wall remains valid for moderately severe pressure gradients, both adverse and favourable (Patel[17]). The departure of the profile from the law of the wall in the outer part is then represented by some weighted addition to the law of the wall, with the weighting dependent (in some generally unknown way) on the upstream history of the layer, being constant for an equilibrium layer. Examples of such approaches are the linear law of Rotta[18] and the wake law of Coles[3]. For boundary layers with injection, it has been shown elsewhere (McQuaid[7]) that the inner law proposed by Stevenson[21] is in very good agreement with the present constant pressure measurements. We might also expect that this inner law would remain valid for moderate pressure gradients with injection and could thus be used as the basis for constructing the overall profile in one or other of the above ways.

The possible representations for the outer profile which could be used to construct a profile family for solid-surface boundary layers were considered by Thompson[28]. He decided to use the intermittency hypothesis of Sarnecki[19] principally because the effects of suction or injection could easily be incorporated at a later stage. He showed that the use of this hypothesis resulted in velocity profiles which agreed very well with solid-surface experiments over a wide range of conditions. In view of Thompson's work, we will here accept the intermittency hypothesis, combined with the inner law of Stevenson, as the method of representing the overall profile. This combination is found to give good predictions of overall velocity profiles when compared to the present data for injection rates up to 0·0145 and to that of Mickley and Davis[16], and Stevenson[22]. The skin-friction law in terms of H and R_θ obtained from the profile family is presented in chart form at five injection rates. Values at any intermediate injection rate can be readily obtained by interpolation.

The auxiliary equation for H is discussed and it is shown that the method of Head[7] based on the entrainment equation gives satisfactory results when extended to layers with injection.

It should be noted that in this Report, all the mean-velocity data of the author's experiments have been corrected for the effects of displacement of the effective centre and of turbulent fluctuations on the reading of pitot probes. The same data tabulated in McQuaid[14] have not been corrected for either of these effects. Coles[4], in a re-examination of boundary-layer data, removed any corrections which had been applied to published data in order to obtain uniformity and, in line with this, the corrections have been omitted in the tabulations.

2. *Establishment of Profile Model using Constant Pressure Measurements.*

2.1. *The Intermittency Hypothesis of Sarnecki.*

The intermittency hypothesis of Sarnecki[19] has been used by Thompson[28] to obtain a velocity profile family for boundary layers on solid surfaces. The hypothesis has been discussed in some detail by Thompson and we will here only outline it briefly before comparing it to the present measurements.

Sarnecki postulated that the observed departure of the velocity distribution from the law of the wall in the outer part of turbulent boundary layers is caused by the intermittently turbulent structure of the layer in this region. The overall time-mean velocity in the intermittent region will be the sum of the mean velocity over the time the flow is turbulent (called u_t) and that over the time the flow is potential (called u_p). If γ is defined as the fraction of the total time for which the flow is turbulent, then the overall time-mean velocity is given by

$$u = \gamma u_t + (1-\gamma)u_p . \tag{2.1.1}$$

The distribution of γ had been obtained from hot-wire anemometer measurements by both Klebanoff[9] and Corrsin and Kistler[5]. No direct measurements of u_p and u_t had been made but Sarnecki assumed that u_p was equal to the local free-stream velocity, i.e.

$$u_p = U_1 . \tag{2.1.2}$$

The experiments of Schubauer[20] had shown that the similarity between the turbulent energy distributions in the wall region of pipes and boundary layers extended also to the outer region if only those parts of the boundary layer which were instantaneously turbulent were considered. Sarnecki assumed that this similarity applied also to the mean velocity, so that u_t is described by the law for the fully turbulent part of the profile. Thus, for solid surface layers,

$$\frac{u_t}{U_\tau} = f\left(\frac{U_\tau y}{\nu}\right) ,$$

$$= A \log_{10} \frac{U_\tau y}{\nu} + B, \text{ for } \frac{U_\tau y}{\nu} > 60. \tag{2.1.3}$$

The distribution of γ can be established experimentally from a mean velocity profile using eqns. (2.1.1) to (2.1.3). Substituting $u_p = U_1$ in eqn. (2.1.1) and re-arranging, we obtain

$$\gamma = \frac{\frac{u}{U_1} - 1}{\frac{u_t}{U_1} - 1} \tag{2.1.4}$$

u/U_1 is the measured (i.e. the overall time-mean) velocity while u_t/U_1 is obtained from fitting the profile to eqn. (2.1.3). By examining a large number of velocity profiles, Sarnecki established that γ was a universal function, being nearly anti-symmetrical about $\gamma = 0{\cdot}5$. He used δ_s to represent the boundary-layer thickness, where δ_s is defined as twice the distance from the wall to the position at which $\gamma = 0{\cdot}5$, so that

$$\gamma = \gamma\,(y/\delta_s). \tag{2.1.5}$$

The distribution of γ can also be established, in principle, from hot-wire anemometer measurements. However, since it is assumed that eqn. (2.1.3) holds throughout the turbulent fluid, the model demands that there will be a discontinuity in velocity at the instantaneous edge of turbulence. This is equivalent to saying that fluid extrained from the potential stream instantaneously reaches turbulent equilibrium, which process will, in practice, require a finite time. It would therefore not be expected that the distributions of γ obtained by the two methods would agree. This is found to be the case so that the two different distributions must be distinguished, the empirical distribution obtained from mean-velocity profiles being denoted by γ_s.

For layers with injection, the inner law of Stevenson, i.e.

$$2\,\frac{U_\tau}{v_o}\left[\left(1+\frac{v_o u}{U_\tau^2}\right)^{\frac{1}{2}} - 1\right] = A\log_{10}\frac{U_\tau y}{\nu} + B, \tag{2.1.6}$$

has been established as the law for the fully turbulent part of the profile (Stevenson[21], McQuaid[15]) and will thus replace eqn. (2.1.3) in the intermittency model. All of the constant-pressure layers in the present series have been analysed to obtain the distribution of γ_s, with u_t/U_1 obtained by fitting Stevenson's inner law to each profile in turn. The values accepted for the constants in eqn. (2.1.6) were $A = 5{\cdot}3$, $B = 5{\cdot}9$, being those which give a best fit to the present measurements. The results are shown in Figs. 1a to e. The single curve shown in these figures is that which best represents the present data; this curve is not the same as that fitted by Thompson[28] to the data analysed by Sarnecki. The two curves are compared in Fig. 2, which also includes the spread about the mean curve originally found by Sarnecki. The present mean curve is seen to be at one extreme of this range. The difference cannot, of course, be attributed to the effect of injection, since the same curve is obtained for the data without injection (*see* Fig. 1a). Sarnecki used slightly different values of the inner-law constants (i.e. $A = 5{\cdot}5$, $B = 5{\cdot}4$) than those used here, but when the data for one of the layers were re-analysed using Sarnecki's choice of constants, the difference in the mean curve obtained was insignificant. Sarnecki did not identify individual sets of measurements in his original correlation for γ_s so that it is not possible to determine whether any consistent differences between different investigations were present. It should, however, be remembered that γ_s (as defined by eqn. (2.1.4)) is the ratio of two (usually) small quantities and the difference in profile shape for the two different distributions would be smaller than appears from Fig. 2. The question of this difference in distributions is returned to when the measurements with pressure gradient are considered.

For the purposes of constructing the profile family and skin-friction law, the mean curve shown in Fig. 1 has been used and is tabulated in Table I.

2.2. *The Profile Family – Comparisons with Experiment.*

In order to complete the description of the overall profile, the law for the sublayer and blending region must now be specified. The law for the viscous sublayer is given by Black and Sarnecki[1] as

$$\frac{u}{U_\tau} = \frac{U_\tau}{v_0}\left(e^{\frac{v_0 y}{\nu}} - 1\right) .$$

No analytical formulation of the law for the blending region between this sublayer law, and the inner law of Stevenson, eqn. (2.1.6), has been attempted. The data obtained here are not sufficiently reliable in this region to enable this to be done, nor indeed to verify that the sublayer law itself is valid. It is therefore assumed that the sublayer law and the inner law each hold on either side of the junction point between the two laws. The errors introduced into the integral profile parameters by this assumption are generally accepted as being insignificant, except perhaps at low Reynolds numbers.

The properties of velocity profiles for constant-pressure layers with injection are now summarised by the universal inner and outer laws, the profile model having the form shown in Fig. 3. For the present data, we use the values $A = 5{\cdot}3$ and $B = 5{\cdot}9$ in the inner law of Stevenson and the distribution of γ_s as tabulated in Table I. The overall velocity profile is therefore given by

$$\frac{u}{U_1} = f\left(\frac{y}{\delta_s}, c_f, R_{\delta_s}, \frac{v_0}{U_1}\right) , \tag{2.2.1}$$

where $R_{\delta_s} = \dfrac{U_1 \delta_s}{\nu}$. The profile family, eqn. (2.2.1), is, for the moment, restricted to constant pressure layers with injection rates no greater than 0·008, since the universality of the distribution of γ_s has only been verified for these limiting conditions. However, for solid surface layers, the intermittency distribution is accepted as being universal for layers in arbitrary pressure gradients, provided that the pressure gradient is not so severe that the semi-logarithmic inner law no longer holds. We would expect the same to be true for combined injection and pressure gradient; comparisons of the profile family with the present pressure gradient measurements will be given in Section 3.

The profile family is not here presented explicitly as was done by Thompson for his solid surface family. The family may be transformed from the form of eqn. (2.2.1) to

$$\frac{u}{U_1} = g\left(\frac{y}{\theta}, H, R_\theta, \frac{v_0}{U_1}\right) , \tag{2.2.2}$$

yielding the two relations

$$c_f = c_f\left(H, R_\theta, \frac{v_0}{U_1}\right) , \tag{2.2.3}$$

$$\text{and } R_{\delta_s} = R_{\delta_s}\left(H, R_\theta, \frac{v_0}{U_1}\right) , \tag{2.2.4}$$

as compatability conditions between eqns. (2.2.1) and (2.2.2). Each of the last two functions was represented in the computer store by an array of H, R_θ covering the experimental range at each injection rate. To obtain comparisons between overall profiles and experiment, the predicted profile from the family at an experimental combination of H and R_θ was found by double interpolation in both these arrays to obtain the corresponding c_f and R_{δ_s}. The profile was then determined from eqn. (2.2.1) and integrated to obtain θ/δ_s and transformed to the more usual co-ordinates u/U_1 *vs.* y/θ.

None of the individual profiles at varying v_0/U_1 which were measured at $U_1 = 30$ and 50 ft/sec was used to obtain the correlation for γ_s. These profiles may thus be used to test the predictions of overall profiles from the family beyond the range of v_0/U_1 used in the correlation for γ_s. Such comparisons have been made for the individual profiles measured at $U_1 = 30$ ft/sec at v_0/U_1 from 0·010 to 0·0143, and are shown in Fig. 4. The agreement is seen to be excellent, the inflected profiles obtained at these injection rates being well represented. Comparisons were also made with some of the profiles of Mickley and Davis, and Stevenson and are shown in Figs. 5, 6 and 7, where the overall agreement is seen to be good. (The experimental H and R_θ used as the basis for comparisons with Mickley and Davis' profiles are recalculated values and not those originally tabulated by them. The integral parameters were obtained using the trapezium rule and the unit Reynolds number was taken as the ratio R_θ/θ as tabulated. The values obtained are considerably different from the tabulated values for some of the profiles at the larger injection rate, but, due to the large scatter on these profiles, the overall level of agreement, or disagreement, with the family would not be significantly affected).

With increasing favourable pressure gradient, the departure from the inner law in the outer region decreases in magnitude and eventually disappears, the inner law then describing the profile almost to the outer edge of the layer. At the extreme outer edge, a negative 'wake component' may appear. Such a state of affairs has been observed by Launder[10], Herring and Norbury[8] and Patel[17] on solid surfaces. Some of the velocity profiles obtained with Pressure Distribution III in the present series with injection are also found to behave similarly when compared with Stevenson's inner law; these comparisons are presented in Section 3.

Under these conditions, the intermittency model can no longer represent the velocity profile, since then u_t may be greater than U_1 for $y < \delta_s$. The limiting condition for physically acceptable profiles from the intermittency model was given by Thompson as $u_t = U_1$ at $y = \delta_s$. At each value of c_f, the upper limit of R_{δ_s} corresponding to this condition is obtained by putting $u_t/U_1 = 1$ in Stevenson's inner law. We thus obtain

$$2\frac{U_\tau}{v_0}\left[\left(1+\frac{v_0}{U_1}\cdot\frac{U_1^2}{U_\tau^2}\right)^{\frac{1}{2}}-1\right] = A\log_{10}\frac{U_\tau\delta_s}{\nu}+B$$

or

$$\log_{10}(R_{\delta_s\ \max.}) = \frac{2}{A}\sqrt{\frac{c_f}{2}}\left[\left(1+\frac{v_0}{U_1}\Big/\frac{c_f}{2}\right)^{\frac{1}{2}}-1\right]\Big/\frac{v_0}{U_1}-\frac{B}{A}-\log_{10}\sqrt{\frac{c_f}{2}}. \tag{2.2.5}$$

A slight difficulty arises with the distribution of γ_s found for the present measurements, since $\gamma_s = 0$ for $y \geqslant 0{\cdot}9\ \delta_s$, rather than $y \geqslant \delta_s$ as in the distribution used by Thompson. The limiting condition for the present distribution must therefore be $u_t = U_1$ at $y = 0{\cdot}9\ \delta_s$, so that the value of $R_{\delta_s\ max.}$ will be greater (by a factor 1/0·9) than that obtained from eqn. (2.2.5).

This limiting condition will be used in the skin-friction law to be described in the next Section.

2.3. *The Skin-Friction Relationship for Layers with Injection.*

The skin-friction relationship in terms of H, R_θ and v_o/U_1, eqn. (2.2.3), has been evaluated at values of $v_0/U_1 = 0$, 0·0025, 0·005, 0·0075 and 0·010 and is shown in Figs. 8a to e. The limiting curve obtained from the condition given in the last Section is also shown in each case. To obtain the skin-friction coefficient at any given pair of H, R_θ, the values of c_f at this combination are read from each chart. When plotted against v_0/U_1, interpolation at the value of v_0/U_1 of interest (if this does not coincide with one of the values in Fig. 8) readily determines c_f. If a large number of such calculations have to be performed, or if c_f is required for $v_0/U_1 > 0{\cdot}010$, the procedure can be programmed for a computer fairly easily, using the choice of A, B and γ_s (y/δ_s) found here.

The present relationship for $v_0/U_1 = 0$ may be compared with that given by Thompson, which was

also obtained using the intermittency model. There are, however, three points on which the present relationship differs from that of Thompson, i.e.

(i) Thompson used van Driest's blending region profile whereas we have assumed the sublayer and inner laws to hold on either side of the junction point, without any such blending region between the two laws;

(ii) he used $A = 5{\cdot}5$, $B = 5{\cdot}4$ whereas we use $A = 5{\cdot}3$, $B = 5{\cdot}9$ as the constants in the inner law and,

(iii) the distributions of γ_s used in the two cases are different.

The skin-friction relationship for Thompson's choice of A, B and $\gamma_s(y/\delta_s)$, but omitting the blending region profile, was evaluated and is compared in Fig. 9 to his original relationship. It is seen that, even at the lowest Reynolds numbers, the effect on the skin-friction law of omitting the blending-region profile is small. Since the proportion of the boundary-layer thickness occupied by the sublayer decreases with increasing injection rate (at constant H, R_θ), this effect will be smaller with injection and can consequently be neglected.

The effect of the change in the inner-law constants, A and B, alone was calculated and found to be even less than that due to the omission of the blending-region profile.

The new relationship for $v_0/U_1 = 0$ is shown compared to that of Thompson in Fig. 10 and to the analytical relationship of Ludwieg and Tillmann[11] i.e.

$$c_f = 0{\cdot}246 \,.\, 10^{-0{\cdot}678H} \,.\, R_\theta \,.^{0{\cdot}268}$$

in Fig. 11. Large differences between Thompson's and the present law occur at large H values and are thus almost entirely due to the different distributions of γ_s used in the two cases, in view of the above findings. The agreement with the Ludwieg and Tillmann law is generally better, being particularly good over the range of H and R_θ in which their law was verified by direct measurements, i.e. $H > 2{\cdot}0$, $3{\cdot}0 < \log_{10} R_\theta < 4{\cdot}3$.

The accuracy of the new skin-friction law will depend on the extent of the universality of the inner and outer profile laws. If the difference in the intermittency distributions found here and by Sarnecki was due to some physical non-similarity, then any law based on the intermittency model will be unreliable at large H values, the maximum unreliability (in one direction) being represented, in view of Fig. 2, by the present relationship. Such large H values will, however, be associated in practice with large adverse pressure gradients or large injection rates, or a combination of these, so that the error in skin-friction coefficient will give rise to only a small error in the calculation of momentum-thickness growth.

A departure from universality of the inner law can be expected to occur when the pressure gradient becomes large and this is discussed in the light of the present measurements with pressure gradient in the next Section.

3. *Boundary Layers with Combined Pressure Gradient and Injection.*

3.1. *General Introduction.*

In practice, the situations where injection would be applied would be those where the skin-friction coefficient, and hence the heat-transfer coefficient, can attain large values. Such large values of skin-friction coefficient are associated with the large favourable pressure gradients that might be obtained in converging ducts or around aerofoil leading edges. It is therefore of some practical importance that the effects of such pressure gradients on the velocity-profile laws, and hence on the skin-friction law, established for constant pressure layers in the last Section, should be examined.

Three boundary layers with combined pressure gradient and injection have been measured by the present author[14]. The velocity distributions for the three layers, designated I, II and III, are shown in Fig. 12. Two of the layers were with moderate gradients of opposite sign and the third with a large favourable gradient. Comparisons with the appropriate laws and a discussion of the effects of pressure gradients in the light of the measurements are given in this Section.

The discussion is necessarily incomplete, however, because of shortcomings in both the experiments and in the theoretical methods available to treat them. In the first case, if an assessment of the effects of

pressure gradient on the inner law were to be attempted similar to that of Patel[17] for solid surface layers, then accurate measurements of shear-stress profiles and skin-friction coefficients are essential and these have not been obtained for the present measurements.

Secondly, if the pressure gradient is large, significant departures from the constant-pressure form of the inner law do occur and a modified form of inner law must be used. Patel has shown that, for solid-surface layers, the mixing-length hypothesis still remains valid under these conditions and the boundary-layer equations, with the pressure-gradient term included, can be integrated to yield a modified inner law. Such a procedure is not, however, possible for injection, since, if both the injection and pressure-gradient terms are included and the mixing-length result is assumed, the boundary-layer equations cannot be solved analytically. For the outer region, Patel also states that both the wake law and the intermittency hypothesis are no longer valid if the modified form of the inner law is used. The overlap argument used by Stevenson[23] to obtain the form of the outer profile for solid surface layers with pressure gradient cannot be extended to the present case, since the method requires the law for the inner profile to be known.

However, the departure with pressure gradient from the constant-pressure form of the inner law is gradual and a fairly wide range of pressure gradients exist for which the unmodified inner law gives acceptable agreement with experiment, as has been shown for solid-surface layers by Thompson[28]. For both of the layers with moderate pressure gradient discussed here, this is also found to be true within the accuracy with which the skin-friction coefficient can be determined from the measurements. For the third layer with large favourable gradient, however, the constant-pressure profile model no longer represents the profile over a significant portion of the layer; for this reason, this layer is discussed separately from the first two layers.

3.2. *The Pressure Gradient Parameter for Layers with Injection.*

Before proceeding to discuss the experiments, it is first necessary to attempt to apply a quantitative measure to the severity of a pressure gradient with injection as far as it affects the inner law. Both Thompson and Patel have used, for solid-surface layers, the parameter Δ_1 which occurs in the expression for the shear-stress distribution, which is, neglecting the acceleration terms,

$$\frac{\tau}{\tau_0} = 1 + \Delta_1 . \eta ,$$

where $\eta = \dfrac{U_\tau y}{\nu}$, $\Delta_1 = \dfrac{\nu}{U_\tau^3} \cdot \dfrac{1}{\rho} \cdot \dfrac{dp}{dx}$. Since the quantity analogous to U_τ for layers with injection is $(U_\tau^2 + v_0 u)^{\frac{1}{2}}$, the modified pressure-gradient parameter can be written as $\dfrac{\nu}{(U_\tau^2 + v_0 u)^{3/2}} \cdot \dfrac{1}{\rho} \dfrac{dp}{dx}$, which we will call Δ_i. Although Δ_i depends on the local velocity u, no great difficulty arises through using a mean value, since the variation of u in the inner turbulent region is small, being no more than about $0{\cdot}1 U_1$.

Since an accurate independent measurement of c_f was not obtained, the values of U_τ used to obtain the Δ_i quoted later were those from the c_f which gave the best fit of Stevenson's inner law to the profiles (including those cases where Stevenson's inner law no longer strictly applies). It will be shown that the behaviour of the inner profile at particular values of Δ_i corresponds satisfactorily to that on a solid surface for the same numerical values of Δ_i.

3.3. *Moderate Pressure Gradients (Pressure Distributions I and II).*

In order to test the validity of Stevenson's inner law, eqn. (2.1.6), the inner-region profile chart, analogous to a Clauser chart for solid-surface boundary layers (Clauser[2]), is constructed for each value of the experimental injection rate. The 'best fit' value of c_f for each profile in turn is determined by plotting the profile on such chart. These values of c_f are then used with the momentum-integral equation to calculate the growth of momentum thickness, θ.

The velocity profiles at alternate x-positions for Pressure Distribution I (moderate adverse pressure gradient) are shown in Fig. 13 and for Pressure Distribution II (moderate favourable pressure gradient) in Fig. 14. In each case, the profile from Stevenson's family which gives a best fit to the experimental profile is shown with the appropriate value of c_f. The values of the inner-law constants used in these comparisons are those found to be appropriate to the present constant-pressure measurements i.e. $A = 5{\cdot}3$, $B = 5{\cdot}9$. It is seen that in all cases the agreement in profile shape is excellent.

For favourable pressure gradients on a solid surface, Patel found that noticeable deviations from the constant pressure inner law did not occur for $\Delta_1 > -0{\cdot}0034$. For adverse pressure gradients, Ludwieg and Tillmann found that for Δ_1 up to at least 0·006, there was again no significant effect. In both these investigations, the skin-friction coefficients were accurately known and so these limiting values can be accepted as reliable. The values of Δ_i for each profile are also shown in Figs. 13 and 14 and they are seen to be within these limits. In view of this, the agreement with the constant pressure inner law is therefore to be expected, if Δ_i is accepted as the parameter corresponding to Δ_1.

The values of c_f found above were used with the momentum-integral equation to calculate the growth of θ in each case. The calculations are shown compared to experiment for Pressure Distribution I in Fig. 15 and for Pressure Distribution II in Fig. 17. Figs. 16 and 18 show the relative magnitudes of the individual terms in the momentum-integral equation. In both cases, it is seen that the effect of errors in the skin-friction coefficient would be a small proportion of $d\theta/dx$. The agreement between the calculated and experimental growths of θ is excellent and is comparable to that obtained for the layers without pressure gradient in McQuaid[15].

The distributions of γ_s for the two layers are shown in Figs. 19a and b. In both cases, the agreement with the curve obtained for constant pressure is good, although some small, but consistent, deviations are apparent; these deviations are discussed in Section 3.5. Comparisons of overall profiles with the present velocity-profile family are shown in Figs. 20 and 21. Again, a small deviation is noticeable for the profiles of Pressure Distribution I, but overall, the agreement can be considered to be very good.

3.4. *Large Favourable Pressure Gradient (Pressure Distribution III).*

The velocity profiles obtained are shown compared with members of Stevenson's inner region family in Figs. 22a and b, together with the values of Δ_i in each case. At the beginning and end of the layer where the pressure gradient was small, members of the family can again be found which will give a good fit to the profiles. For the intermediate four measuring stations (from $x = 21{\cdot}8$ in. to $x = 30{\cdot}8$ in.) the profiles appear to deviate from the family in the same way as noted by Patel on a solid surface. Patel found that for the range $-{\cdot}0034 > \Delta_1 > -{\cdot}0245$, the measured velocity profile falls below the constant pressure inner law and shows the trends predicted by the modified inner law mentioned in Section 3.1. In Patel's experiments the values of c_f were accurately known. Here, this is not the case and we simply show in each case the member of Stevenson's family which gives qualitative agreement with the observation of Patel. It is seen that the deviation from the constant-pressure law occurs (except for $x = 17{\cdot}0$ in.) at values of Δ_i which are in agreement with the limiting value of $\Delta_1 = -0{\cdot}0034$ given by Patel.

Notwithstanding that the values of c_f are in doubt for the intermediate stations, the best fit values of c_f were again used to calculate the growth of θ and the result is shown compared with experiment in Fig. 23. The individual terms in the momentum-integral equation are shown in Fig. 24. Again the magnitude of $c_f/2$ is much less than either the injection or pressure-gradient terms, but its influence is now greater than in the previous two layers. Over the greater part of the layer, the injection and pressure-gradient terms almost balance and errors in c_f would then have a significant effect on $d\theta/dx$, so that the agreement between the calculated growth of θ and experiment must be considered good.

From Fig. 25, it is clear that the intermittency model is no longer valid for the profiles between $x = 21{\cdot}8$ in. and $x = 30{\cdot}8$ in. Irrespective of the choice of curve fitted to the inner part of the profile, it is seen that the local velocity near the outer edge becomes less than the turbulent fluid velocity, u_t, given by such a fitted curve. These profiles are therefore excluded from the profile family by the limiting condition on the skin-friction law given in Section 2.3. Comparisons of the profile family with those profiles for which the inner region is satisfactorily described by the constant pressure inner law are shown in Fig.

25, where the agreement is seen to be good.

It is interesting to note that the intermediate profiles resemble those measured with an asymptotic layer with suction by Tennekes[24]. In that layer, $d\theta/dx$ is zero and the inner law given by Tennekes describes almost the whole profile, with a small wake component at the outer edge. Here, $d\theta/dx$ is also approximately zero (being, in fact, slightly negative over the mid-part of the layer) and it is seen from Fig. 22 that the inner greater part of the profile. This also accords with the velocity defect law given in McQuaid[13], which states that when $d\theta/dx$ falls to zero the 'outer region' disappears.

3.5. *Discussion on the Universality of the Intermittency Distribution.*

For the same range of the modified parameter Δ_i as for Δ_1 on a solid surface, the constant-pressure inner law of Stevenson has been found to agree with experiment within the accuracy with which c_f could be determined. The distribution of γ_s, however, shows some slight deviations from universality with pressure gradient and these are now discussed in more detail.

Referring to Fig. 19a, it is seen that the data for the adverse pressure-gradient layer depart consistently from the constant-pressure curve in a direction such that improved agreement with the mean curve of Thompson (shown in Fig. 2) is obtained. For adverse gradients on a solid surface, the effect of the pressure gradient on the inner law manifests itself as a deviation at the outer edge of the inner region. It is still found that the velocity profile over part of the inner region can be matched to a member of the constant-pressure inner-law family of profiles. With increasing Δ_1, the extent of the profile described by the inner law decreases until eventually no straight line portion can be obtained. With such behaviour, the distribution of γ_s will also be affected, the point of departure from $\gamma_s = 1$ moving to lower values of y/δ_s as Δ_1 increases. Thompson[28] has observed that the mean curve for γ_s used by him did not give very good agreement for velocity profiles near to separation and he pointed out that an improved level of agreement would have been obtained if the point of departure from $\gamma_s = 1$ had been at $y/\delta_s = 0$, as is effectively the case with Coles' wake law. For moderate favourable gradients, the opposite is true, the inner law holding through a greater part of the profile than with constant pressure. There should thus be a consistent trend of the γ_s distribution with variation of Δ_1 or Δ_i.

Thompson's mean curve for γ_s was obtained from the data analysed by Sarnecki, which were almost entirely confined to adverse pressure-gradient profiles, only one constant-pressure profile and one favourable gradient profile from the experiments of Ludwieg and Tillmann being included. Thompson's choice of mean curve will therefore be weighted towards adverse pressure-gradient conditions and constant-pressure results will fall at one extreme of the range (as happens with the present constant-pressure data), with near-separation profiles at the other extreme. The present adverse pressure-gradient results do tend towards agreement with Thompson's mean curve, thus supporting the above argument.

This lack of complete universality in the γ_s distribution is the cause of the rather large differences noted between the present skin-friction law and that of Thompson at large values of H. The present law will be in error in adverse-gradient conditions, whereas Thompson's should give a satisfactory averaging over the range from constant pressure to near-separation, as indeed he showed by the profile comparisons he made.

For the moderate favourable gradient, the distribution of γ_s in Fig. 19b is seen to deviate from the constant-pressure curve near the outer edge of the layer. The trend in Fig. 19b is in agreement with the observation of Thompson that the predicted profiles using the intermittency model will give too slow an approach to the free stream as the limiting condition given in Section 2.3 is approached. Thompson somewhat extended the range of his family in these conditions by a velocity defect argument for the outer edge of the profile, but this has not been attempted here.

The above limitations are inherent in the two parameter representation of the profile adopted here. This representation does, however, appear to give results of acceptable accuracy for conditions where the constant-pressure inner law is valid over a significant part of the inner region. The introduction of a third (pressure gradient) parameter which would account for the extent of the region of validity of the inner law would greatly increase the complexity of the model and does not at present seem warranted.

4. *Boundary Layer with a Discontinuity in the Injection Velocity Distribution.*

4.1. *Qualitative Features.*

There may be cases in practice where injection might usefully be confined only to those regions where high values of wall shear stress occur. At the upstream and downstream ends of such a region, the boundary layer will be in a non-equilibrium state while adjusting from one regime to the other. The remarks which were made in Section 1 regarding the differing response of the inner and outer parts of the layer in non-equilibrium conditions should apply in such a case. Three distinct regimes may be identified in the region downstream of the change in surface condition:

(i) Immediately downstream, the acceleration terms in the boundary-layer equations will be large, so that the usual inner-region approximations and hence the usual forms of inner law do not apply. Because of the rapid response of the inner region, this regime would be expected to extend to only a few boundary-layer thicknesses downstream and will be referred to as the *transient* regime.

(ii) This will be followed by an *intermediate* region where the constant stress inner law will hold. The behaviour of the layer would then be expected to be the same as with non-equilibrium pressure gradients, in that, although the outer profile will still be responding slowly to the imposed change, the departure from the inner law in the outer region will display a nearly universal form. The overall velocity profile in this region would then be a member of the velocity-profile family. The slow response of the outer part will mean that a considerable distance may elapse before

(iii) the *fully developed state* is attained, where equilibrium relationships will be satisfied by the overall profile. For constant-pressure layers on a solid surface, these equilibrium relationships would be the von Karman velocity-defect law or the unique H *vs.* R_θ curve.

The first of the above regions will be important if the injection velocity is distributed in discrete spanwise strips, where, depending on the geometry of the strips, the inner part of the layer may not have fully adjusted to the local surface condition between each successive change of conditions.

We here, however, confine our attention to the relatively simple case where the width of the strips is such that the boundary layer is permitted to re-adjust to the fully-developed state between each successive strip. In particular, we consider only the boundary layer re-adjusting from the fully-developed injection state to the fully-developed solid surface state in zero pressure gradient. Measurements have been made on such a layer where the injection rate changed from 0·0034 to nearly zero, and, in the following Section, these measurements are compared to the predictions of the profile family. The measurements suffered from a number of inadequacies which are fully discussed in McQuaid[14]. In particular, there was a small residual injection rate over the nominally zero injection part of the layer; in the comparisons to follow, this injection rate is neglected.

4.2. *Comparisons with the Profile Family and a Discussion on the Length Scale of the Adjustment Region.*

The overall velocity profiles upstream of the discontinuity are compared with the present profile family in Fig. 26 where it is seen that the agreement is good. (The slight disagreement in profile shape which is apparent in Fig. 26 can be attributed to the absence of a blending region in the profile model).

The overall velocity profiles downstream of the discontinuity are compared with the family in Figs. 27a and b. (In this and the following figures, the distance from the discontinuity is given by $x-x_0$; the discontinuity occurs at $x = x_0 = 17{\cdot}5$ in. from the leading edge of the plate). For these members of the profile family, an approximate form of bledning-region profile has been included. The lack of agreement between the profile family and experiment which would be apparent at these comparatively low Reynolds numbers if the blending-region profile was omitted would obscure the effects of the non-equilibrium conditions. The blending-region profile used was obtained from the zero injection data of the main experiments and, to an accuracy sufficient for the present purposes, could be represented by a simple linear-logarithmic law connecting the sublayer and inner laws, with the coefficients

$$\frac{u}{U_\tau} = 10{\cdot}2 \log_{10} \frac{U_\tau y}{\nu} - 2{\cdot}2.$$

It is seen from Fig. 27 that the overall profile adjusts quite rapidly to the change in the wall condition when viewed in this way. The profiles can be considered to be members of the family for $x-x_0 \geqslant 4$ in., i.e. for distances greater than about 8 boundary-layer thicknesses from the discontinuity. The layer itself has not, however, returned to the fully-developed state even at the last measuring station, in that the H, R_θ values do not conform to the zero injection, zero pressure-gradient mean curve obtained from the data of the main experiments, as is shown in Fig. 28. Fig. 29 shows the $c_f/2$ obtained from Preston tube readings, using Patel's calibration, compared to the zero injection and zero pressure-gradient curve and they are seen to agree for $x-x_0 \geqslant 7{\cdot}5$ in. (In both Figs. 28 and 29, the curves from the main experiments have had to be extrapolated to the slightly higher Reynolds numbers of the present experiment, as shown by the broken lines). The differing behaviour of H and the Preston tube c_f demonstrates, as would be expected, that the inner region returns to equilibrium much faster than the outer region.

This experiment shows that the fully-developed state is not quite reached even at the last measuring station, 33 boundary-layer thicknesses downstream from the discontinuity. In the main experiments, it was accepted that the fully-developed injection state is reached at $x = 11{\cdot}5$ in. which corresponds to about 40 boundary-layer thicknesses downstream from the beginning of injection. Thus, in the light of the present result, this may not be fully justified. This should not affect any of the conclusions concerning the velocity-profile laws, since the fully-developed profile model should again hold for distances greater than about 8 boundary-layer thicknesses from the onset of injection. A small error will be present in the initial H value for calculations of H development, but as shown by Thompson[26] this has little effect on the subsequent calculation using Head's[7] equation with which, in the next Section, we will be particularly concerned.

The first five profiles downstream from the discontinuity are plotted in Clauser plot form in Fig. 30, with the constants $A = 5{\cdot}3$, $B = 5{\cdot}9$. For $x-x_0 = 4$ in. (and for all the subsequent profiles, not shown in Fig. 30) the inner profile can be fitted very well by a member of the semi-logarithmic inner-law family. This downstream distance is the same as found from the overall profile comparisons, but differs (by one measuring station) from that obtained from the Preston-tube results. We can conclude that, where the inner profile can be fitted by the inner law, the intermittency model describes the overall profile, even though the layer has not returned to the equilibrium or fully developed state. The behaviour is thus the same as that found in Section 3 for non-equilibrium pressure gradients.

In the transient regime ($x-x_0 \leqslant 1{\cdot}6$ in.), the inner-region profiles in Fig. 30 are seen to disagree with the inner law in the same manner as for large adverse pressure gradients on a solid surface (Patel[17]). An inner law of the same form as that obtained by Townsend[29], for the case of pressure gradients where the acceleration term in the shear-stress distribution is appreciable, could be used to fit these velocity profiles. This law uses a linear approximation to the shear-stress distribution and, for the present case, only the term containing the effect of $\dfrac{d\tau_0}{dx}$ would be included. To test such an hypothesis adequately, the distribution of c_f would need to be known accurately and this is not the case for the present data. We can, however, conclude that, as for the case of large adverse pressure gradients on a solid surface, the constant-stress law used as the basis for the profile family will predict skin-friction coefficients which will be too large in this region. For the region downstream of the beginning of injection, the prediction will be too small. A quantitative assessment of this error would require more accurate data than is at present available. For distances greater than about 8 boundary-layer thicknesses from a discontinuity, the skin-friction law should, however, give an accurate prediction of the skin-friction coefficient.

5. *The Calculation of Shape-Factor Development for Boundary Layers with Injection.*

A variety of auxiliary equations have been proposed for solid-surface layers, the better known examples being based either on the kinetic energy equation (e.g. Truckenbrodt[30] and Escudier and Spalding[6]), the moment-of-momentum equation (McDonald and Stoddart[12]) or the entrainment equation (Head[7] and Thompson[27]). Irrespective of the approach, some degree of empiricism will be involved e.g. for the dissipation integral and the shape factor H_ε in methods based on the kinetic energy equation, or for the entrainment rate and the shape factor $H_{\delta-\delta^*}$ in the entrainment equation. In principle, the extension of

any of the above methods to the case of injection would require fresh knowledge of these quantities to be obtained for the new conditions. Those relations which depend on the overall profile shape (i.e. H_ε *vs.* H or $H_{\delta-\delta^*}$ *vs.* H, with a dependence also on R_θ if a two-parameter family is assumed) can most easily be established if the properties of the velocity profiles with injection are summarised in a profile family. However, it would be expected that these relations would not be significantly affected by injection, in that they relate geometrical properties of reasonably well-behaved curves with specified boundary conditions. This is seen to be the case in Figs. 31 and 32 where calculations of $H_{\delta-\delta^*}$ and H_ε *vs.* H for some of the present data are shown compared with the curves obtained by Thompson from his solid surface profile family. The data shown fell within the range of R_θ from 2×10^3 to 10^4; the agreement with the solid-surface results is seen to be excellent.

Thompson[25] pointed out that the overall dissipation in the layer is likely to be strongly influenced by the change in conditions at the wall, so that the solid-surface correlation for the dissipation integral might not be suitable for use with suction or injection. He noted that the entrainment process should not be so affected, so that auxiliary equations based on the entrainment hypothesis then simply require an additive term to include the effect of injection. Both Head and Thompson showed that calculations of H for some of the layers with injection measured by Mickley and Davis[16], using the solid-surface auxiliary equation modified in this way, were in good agreement with experiment. In addition, Thompson[26] showed that, of the better known equations, Head's equation gave consistently the best agreement with experiment for solid-surface layers. In view of this, we will confine our attention to this particular equation. Comparisons between calculations using Head's equation (with the experimental distribution of momentum thickness, θ) and experimental shape-factor developments are shown in Figs. 33a to e. It is seen that, with the possible exception of the layer with Pressure Distribution III, the agreement between calculation and experiment can be considered very satisfactory. In particular, for the layer with a discontinuity in the injection rate, where H decreases along the layer, the agreement is very good.

6. *Conclusions.*

(i) The extension to boundary layers with injection of the intermittency hypothesis of Sarnecki, using the inner law of Stevenson to represent the velocity distribution in the turbulent fluid, gives results which are in excellent agreement with the constant-pressure measurements of this investigation up to $v_0/U_1 = 0{\cdot}0143$ and with those of Mickley and Davis, and Stevenson.

(ii) The distribution of the intermittency, γ_s, for the present measurements has been found to differ from that used by Thompson. From the behaviour observed for the present data with pressure gradient, it was concluded that this difference is most likely due to a weighting of Thompson's distribution to adverse pressure-gradient conditions. This departure from universality with pressure gradient is small, however, and the model gives very good predictions of overall velocity profiles with combined pressure gradient and injection, provided the inner law of Stevenson is still reliable. It was concluded that this condition is satisfied if the pressure-gradient parameter,

$$\Delta_i = \frac{\nu}{\rho\,(U_\tau^2 + v_0 u)^{3/2}} \frac{dp}{dx}$$

is within the limits $-{\cdot}004 < \Delta_i < {\cdot}006$; Δ_i is the analogue of the parameter $\Delta_1 = \dfrac{\nu}{\rho U_\tau^3} \dfrac{dp}{dx}$ used by Thompson and Patel as a measure of the severity of a pressure gradient on solid surfaces.

(iii) After a sudden change in injection rate, it was found that the profile model does not represent the velocity profile in the region within about 8 boundary-layer thicknesses downstream from the change. The skin-friction law will be in error in this region and will tend to overestimate the skin friction for the case where the injection rate falls and *vice versa.* It was found that the fully-developed state was not attained even at 33 boundary-layer thicknesses downstream from the change.

(iv) The auxiliary equation of Head has been found to give satisfactory predictions of shape-factor development for the range of conditions covered by the present measurements.

(v) The new skin-friction law and the auxiliary equation of Head should, with the momentum-integral equation, provide a satisfactory means of calculating boundary-layer development with both injection and pressure gradient.

7. *Acknowledgement.*

The author wishes to acknowledge the generous advice and encouragement he has received from his supervisor, Dr. L. C. Squire, during the course of this work.

LIST OF SYMBOLS

A,B	Constants in the semi-logarithmic inner law $\left(A = \frac{1}{\kappa}\log_e 10\right)$
c_f	Local value of the skin-friction coefficient $\left(= \frac{\tau_0}{\frac{1}{2}\rho U_1^{\,2}}\right)$
f, g	Used to denote functional dependence
$H, H_{\delta-\delta^*}, H_\varepsilon$	Profile shape-factors: $H = \frac{\delta^*}{\theta}$; $H_{\delta-\delta^*} = \frac{\delta-\delta^*}{\theta}$; $H_\varepsilon = \frac{\varepsilon}{\theta}$
p	Static pressure
R_θ, R_{δ_s}	Reynolds numbers: $R_\theta = \frac{U_1\theta}{\nu}$; $R_{\delta_s} = \frac{U_1\delta_s}{\nu}$
$R_{\delta_s \max}$	Limiting value of R_{δ_s}
u,v,w	Components of velocity in the boundary layer in the x, y and z directions respectively
u_p	Mean velocity of the potential fluid over 'time potential'
u_t	Mean velocity of the turbulent fluid over 'time turbulent'
U_1	Free stream velocity
U_{ref}	Value of U_1 at reference position
U_τ	Wall shear velocity $\left(= (\frac{\tau_0}{\rho})^{\frac{1}{2}}\right)$
v_0	Transpiration velocity at the wall (positive for injection)
x,y,z	Space co-ordinates along, normal to, and across the surface
γ, γ_s	Intermittency factors (defined in the text)
δ_s	Definition of boundary-layer thickness: $\delta_s = 2(y$ at $\gamma_s = \cdot 5)$

δ^* Displacement thickness $= \int_0^\infty (1-\frac{u}{U_1})\,dy$

Δ_1 $= \frac{\nu}{\rho U_\tau^3}\frac{dp}{dx}$

Δ_i $= \frac{\nu}{\rho(U_\tau^2+v_0 u)^{3/2}}\frac{dp}{dx}$

ε Energy loss thickness $= \int_0^\infty \left(1-(\frac{u}{U_1})^2\right)\frac{u}{U_1}\,dy$

η $= \frac{U_\tau y}{\nu}$

θ Momentum loss thickness $= \int_0^\infty (1-\frac{u}{U_1})\frac{u}{U_1}\,dy$

κ Mixing-length constant

μ Coefficient of viscosity

ν Kinematic viscosity

ρ Fluid density

τ Shear stress $= \mu\frac{\partial u}{\partial y} - \rho\,\overline{u'v'}$

τ_0 Wall shear stress

REFERENCES

No.	Author(s)	Title, etc.
1	T. J. Black and A. J. Sarnecki	The turbulent boundary layer with suction or injection. A.R.C. R & M 3387. October 1958.
2	F. H. Clauser	Turbulent boundary layers in adverse pressure gradients. *J. Aeronaut. Sci.*, Vol. 21, No. 2, pp. 91–108. 1954.
3	D. Coles	The law of the wake in the turbulent boundary layer. *J. Fluid Mech.*, Vol. 1, pt. 2, pp. 191–226. 1956.
4	D. Coles	The turbulent boundary layer in a compressible fluid. Rep. for U.S.A.F. Project Rand, R–403–PR. 1962.
5	S. Corrsin and A. L. Kistler	The free-stream boundaries of turbulent flows. NACA Rep. 1244, 1955 (formerly NACA TN 3133).
6	M. P. Escudier and D. B. Spalding	A note on the turbulent uniform-property hydrodynamic boundary layer on a smooth impermeable wall; comparisons of theory with experiment. A.R.C. C.P. 875. 1965.
7	M. R. Head	Entrainment in the turbulent boundary layer. A.R.C. R & M 3152. September 1958.
8	H. J. Herring and J. F. Norbury	Some experiments on equilibrium turbulent boundary layers in favorable pressure gradients. Princeton Univ. AMS Rep. FLD No. 15.
9	P. S. Klebanoff	Characteristics of turbulence in a boundary layer with zero pressure gradient. NACA Rep. 1247, 1955 (formerly NACA TN 3178, 1954).
10	B. E. Launder	The turbulent boundary layer in a strongly negative pressure gradient. M.I.T. Gas Turbine Lab. Rep. No. 71. 1963.
11	H. Ludwieg and W. Tillmann	Investigation of the wall shearing stress in turbulent boundary layers. NACA TM 1285, 1950.
12	H. McDonald and J. A. P. Stoddart	On the development of the incompressible turbulent boundary layer. British Aircraft Corporation Rep. No. Ae 225; A.R.C. R & M 3484. January 1966.
13	J. McQuaid	A velocity defect relationship for the outer part of equilibrium and near-equilibrium turbulent boundary layers. A.R.C. C.P. 885. October 1965.
14	J. McQuaid	Experiments on incompressible turbulent boundary layers with distributed injection. A.R.C. 28 735. January 1967.
15	J. McQuaid	A note on the inner turbulent region of boundary layers with distributed injection. To be published.

No.	Author(s)	Title, etc.
16	H. S. Mickley and R. S. Davis	Momentum transfer for flow over a flat plate with blowing. NACA TN 4017. 1957.
17	V. C. Patel	Contributions to the study of turbulent boundary layers. Ph.D. dissertation, Cambridge University. 1965.
18	J. C. Rotta	On the theory of the turbulent boundary layer. NACA TM 1344. 1953.
19	A. J. Sarnecki	The turbulent boundary layer on a permeable surface. Ph.D. dissertation, Cambridge University. 1959.
20	G. B. Schubauer	Turbulent processes as observed in boundary layer and pipe. *J. App. Phys.*, Vol. 25, pp. 188–196. 1954.
21	T. N. Stevenson	A law of the wall for turbulent boundary layers with suction or injection. A.R.C. 26 025. July 1963.
22	T. N. Stevenson	Experiments on injection into an incompressible turbulent boundary layer. A.R.C. 26 989. October 1964.
23	T. N. Stevenson	The mean flow in the outer region of turbulent boundary layers. AGARDograph 97, pt. 1, pp. 281–314. 1965.
24	H. Tennekes	Similarity laws for turbulent boundary layers with suction or injection. *J. Fluid Mech.*, Vol. 21, pt. 4, pp. 689–703. 1965.
25	B. G. J. Thompson	The calculation of turbulent boundary layers. Ph.D. dissertation, Cambridge University.
26	B. G. J. Thompson	A critical review of existing methods of calculating the turbulent boundary layer. A.R.C. R & M 3447. August 1964.
27	B. G. J. Thompson	The calculation of shape-factor development in incompressible turbulent boundary layers with or without transpiration. AGARDograph 97, pt. 1, pp. 159–197. 1965.
28	B. G. J. Thompson	A new two-parameter family of mean velocity profiles for incompressible turbulent boundary layers on smooth walls. A.R.C. R & M 3463. April 1965.
29	A. A. Townsend	Equilibrium layers and wall turbulence. *J. Fluid Mech.*, Vol. 11, pt. 1, pp. 97–120. 1960.
30	E. Truckenbrodt	A method of quadrature for calculation of the laminar and turbulent boundary layer in the case of plane and rotationally symmetric flow. NACA TM 1379, 1955.

TABLE 1

Distribution of γ_S Accepted for the Present Data.

y/δ_s	γ_s
0	1·000
·13	1·000
·15	·992
·175	·979
·2	·961
·25	·915
·3	·855
·35	·782
·4	·696
·45	·600
·5	·500
·55	·400
·6	·304
·65	·215
·7	·137
·75	·073
·8	·033
·85	·012
·9	0
1·0	0

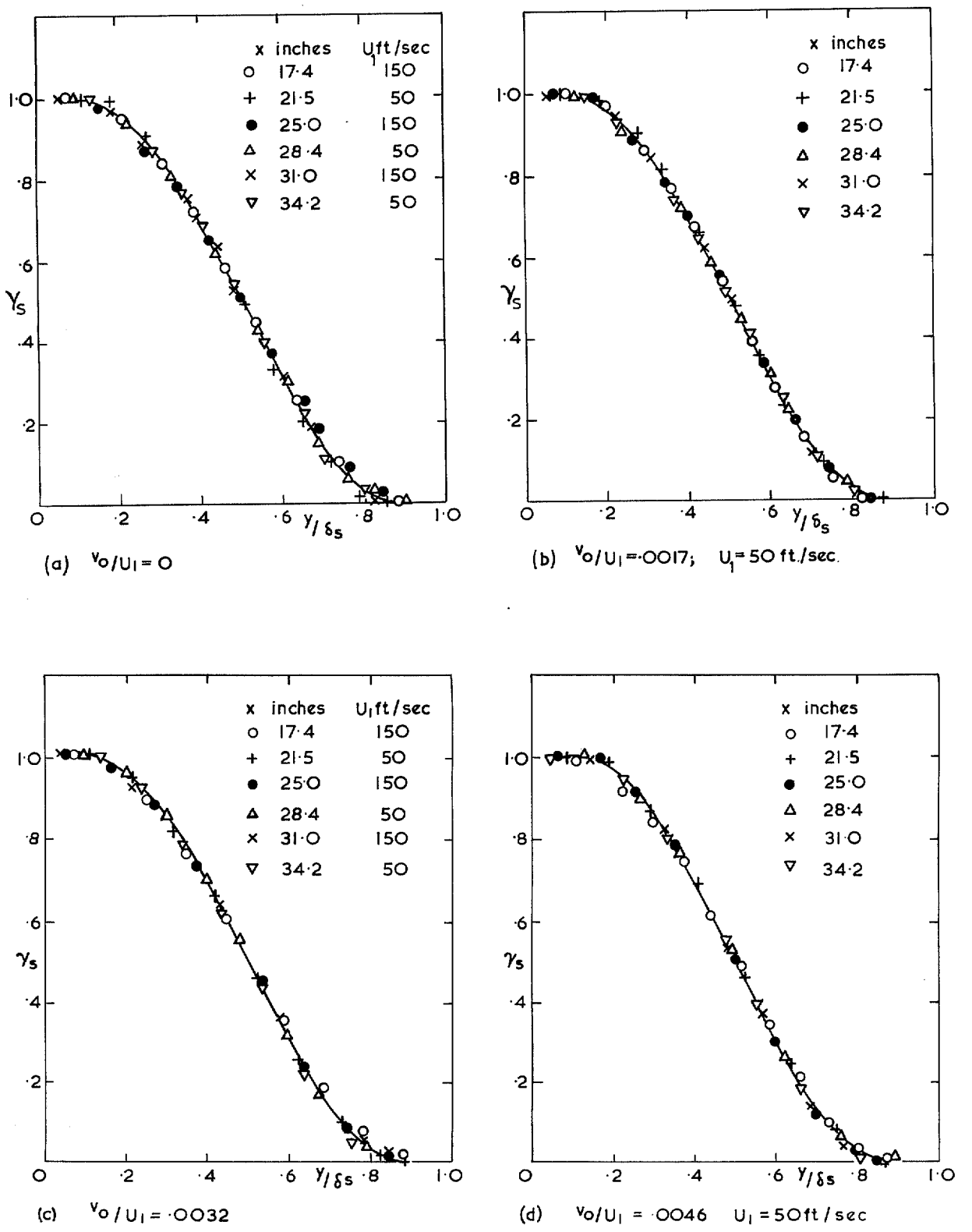

FIG. 1. Comparison of intermittency hypothesis with experiment.

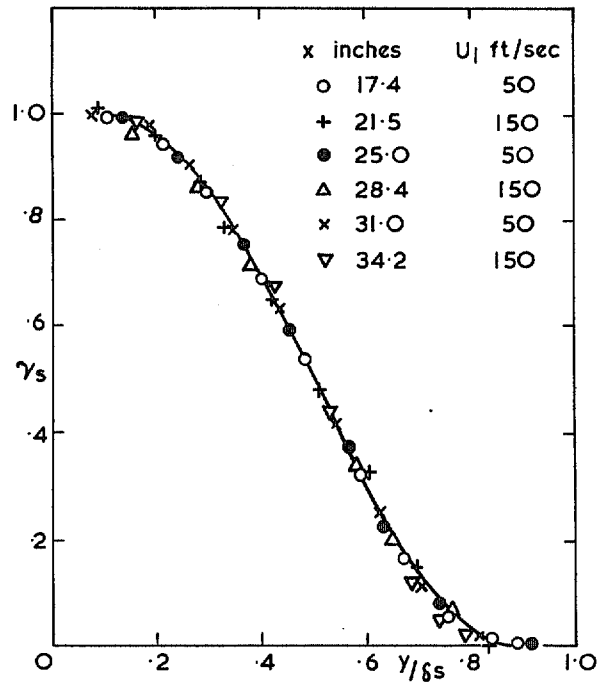

(e) $v_o/U_1 = \cdot 008$

FIG. 1 (concl.). Comparison of intermittency hypothesis with experiment.

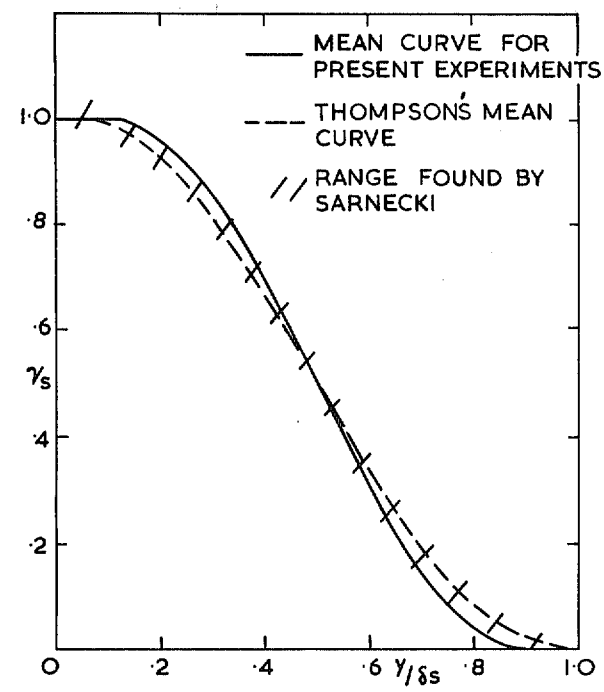

FIG. 2. Comparison of alternative intermittency distributions.

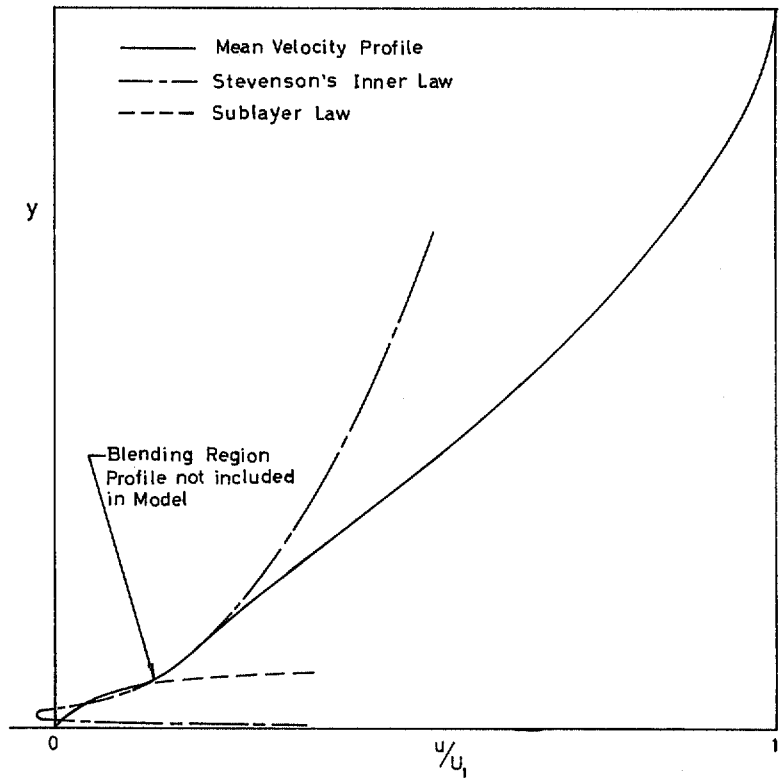

FIG. 3. Velocity-profile model.

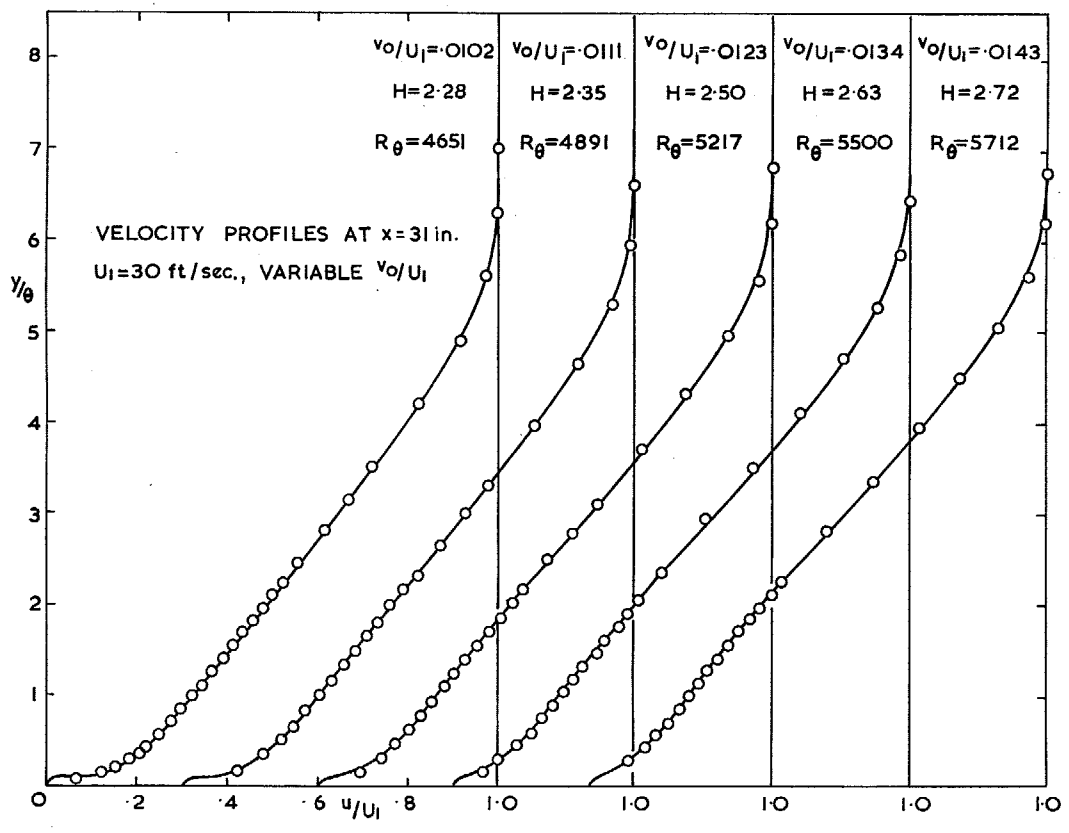

FIG. 4. Comparison of the profile family with experiment.

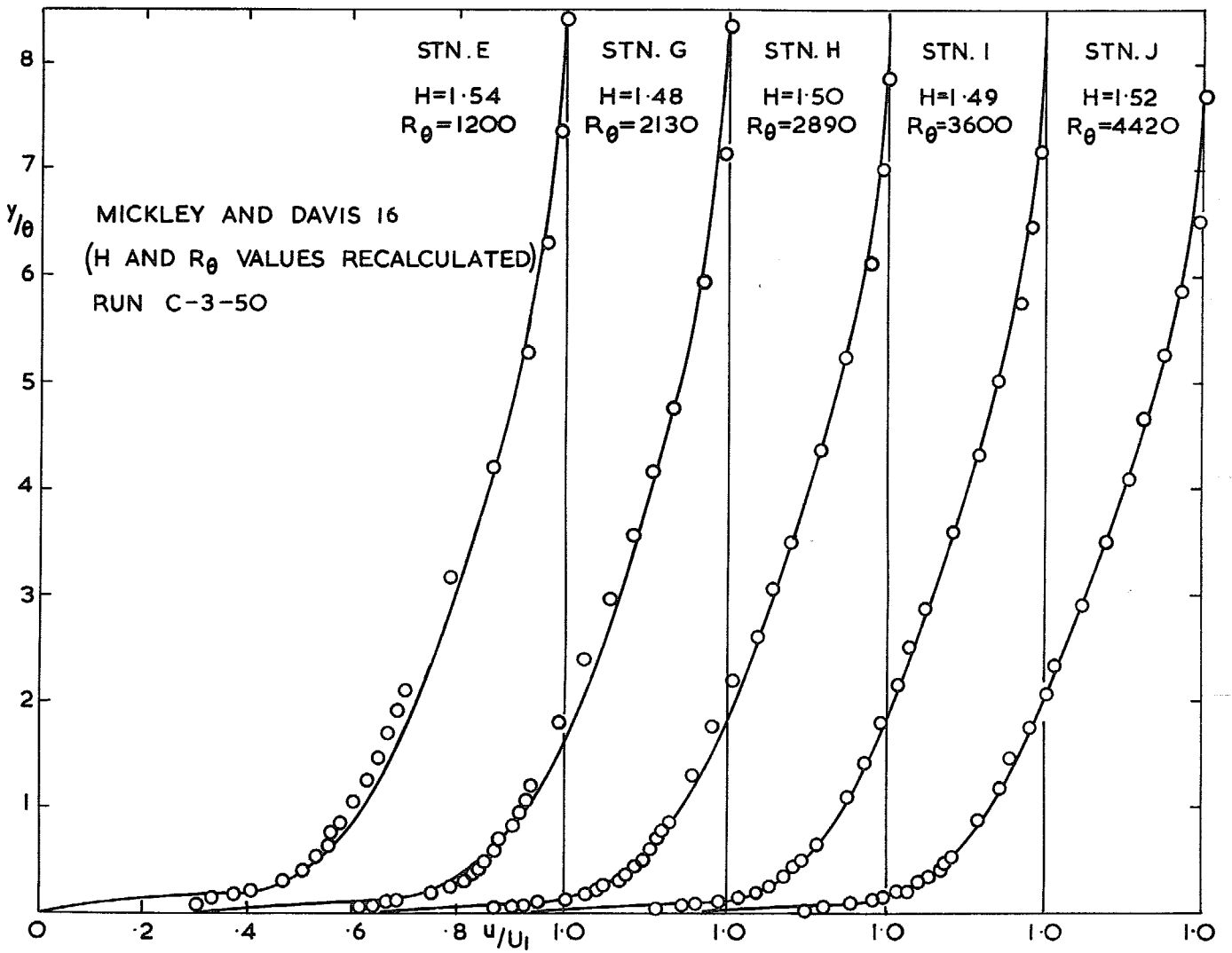

FIG. 5. Comparison of the profile family with experiment.

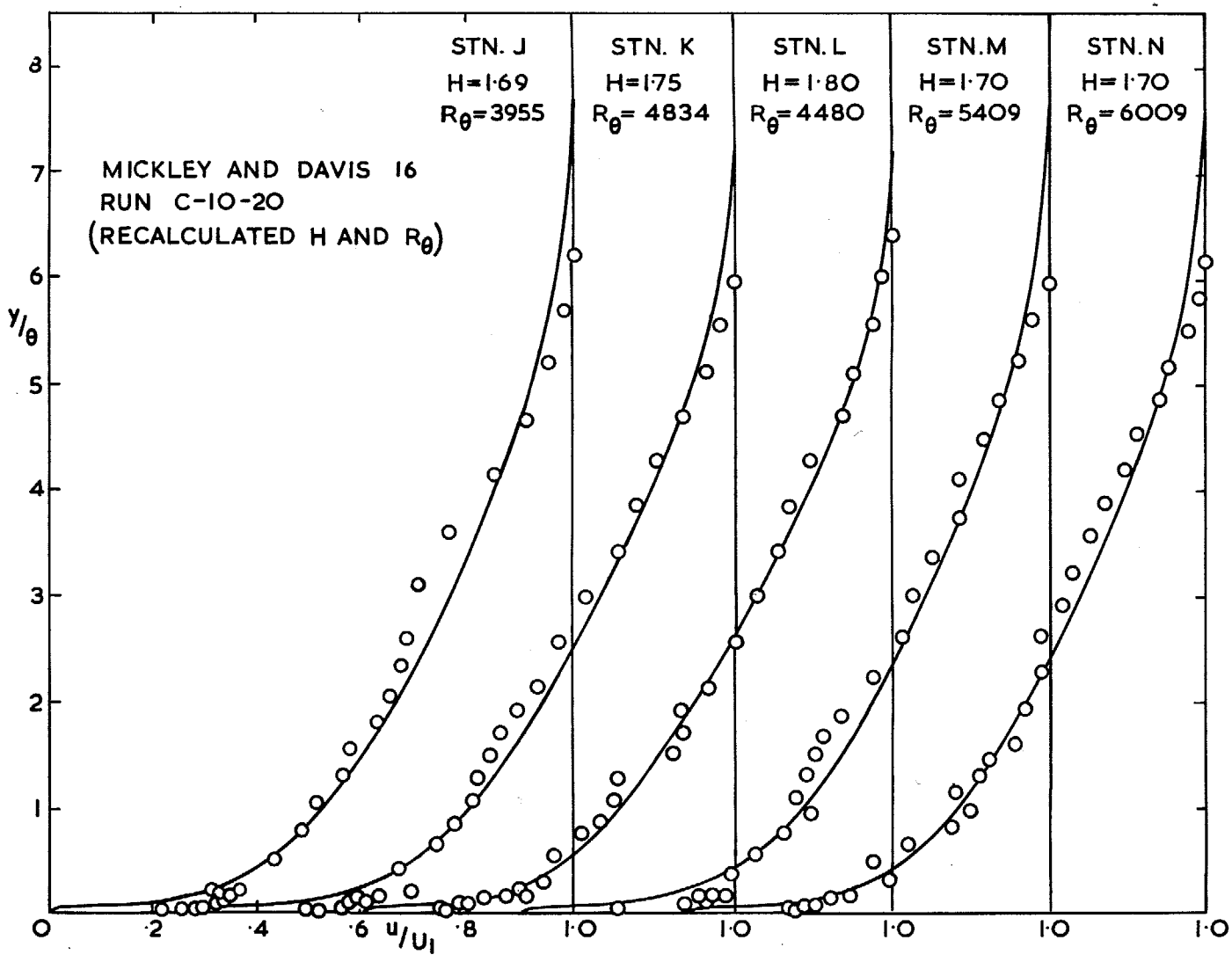

FIG. 6. Comparison of the profile family with experiment.

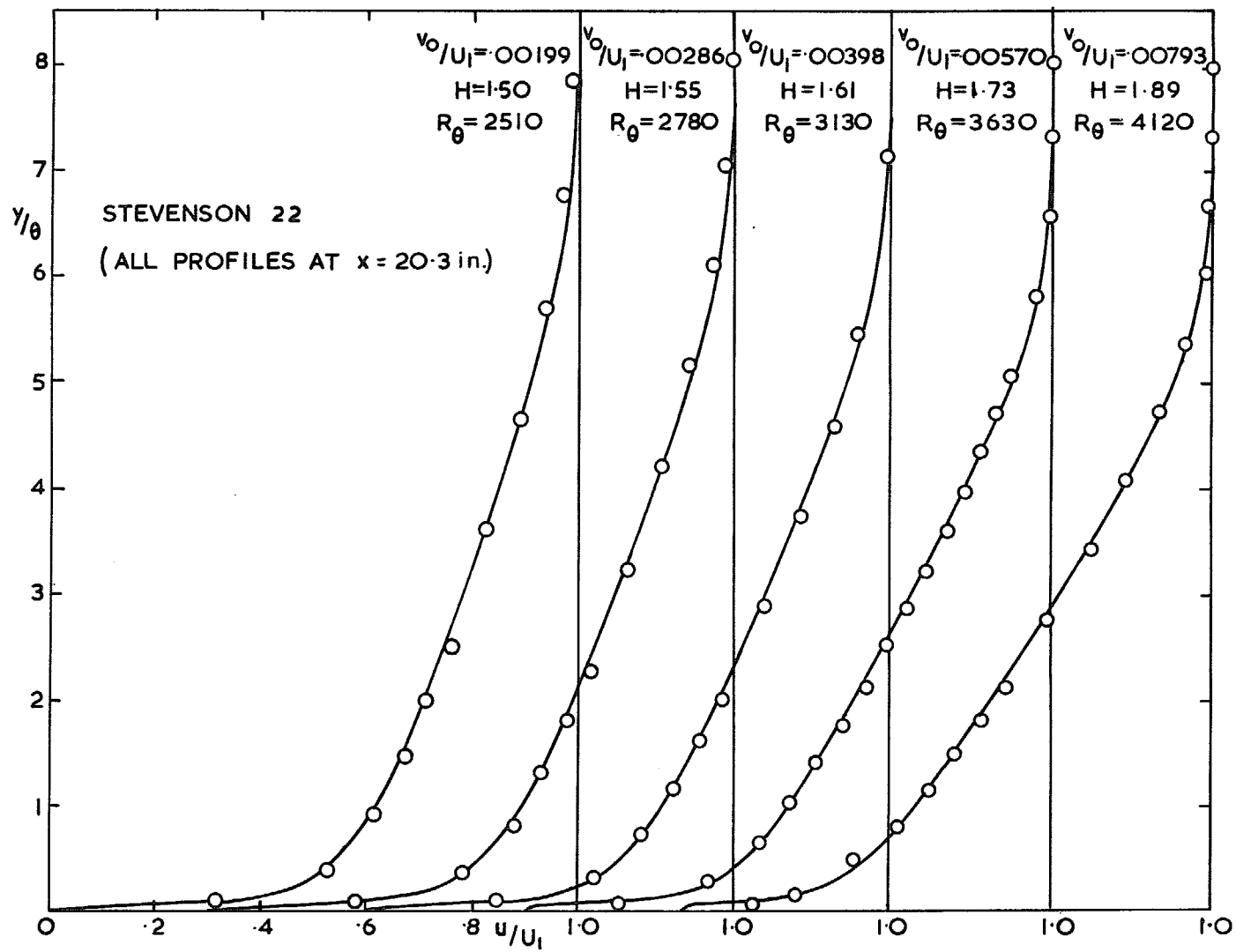

FIG. 7. Comparison of the profile family with experiment.

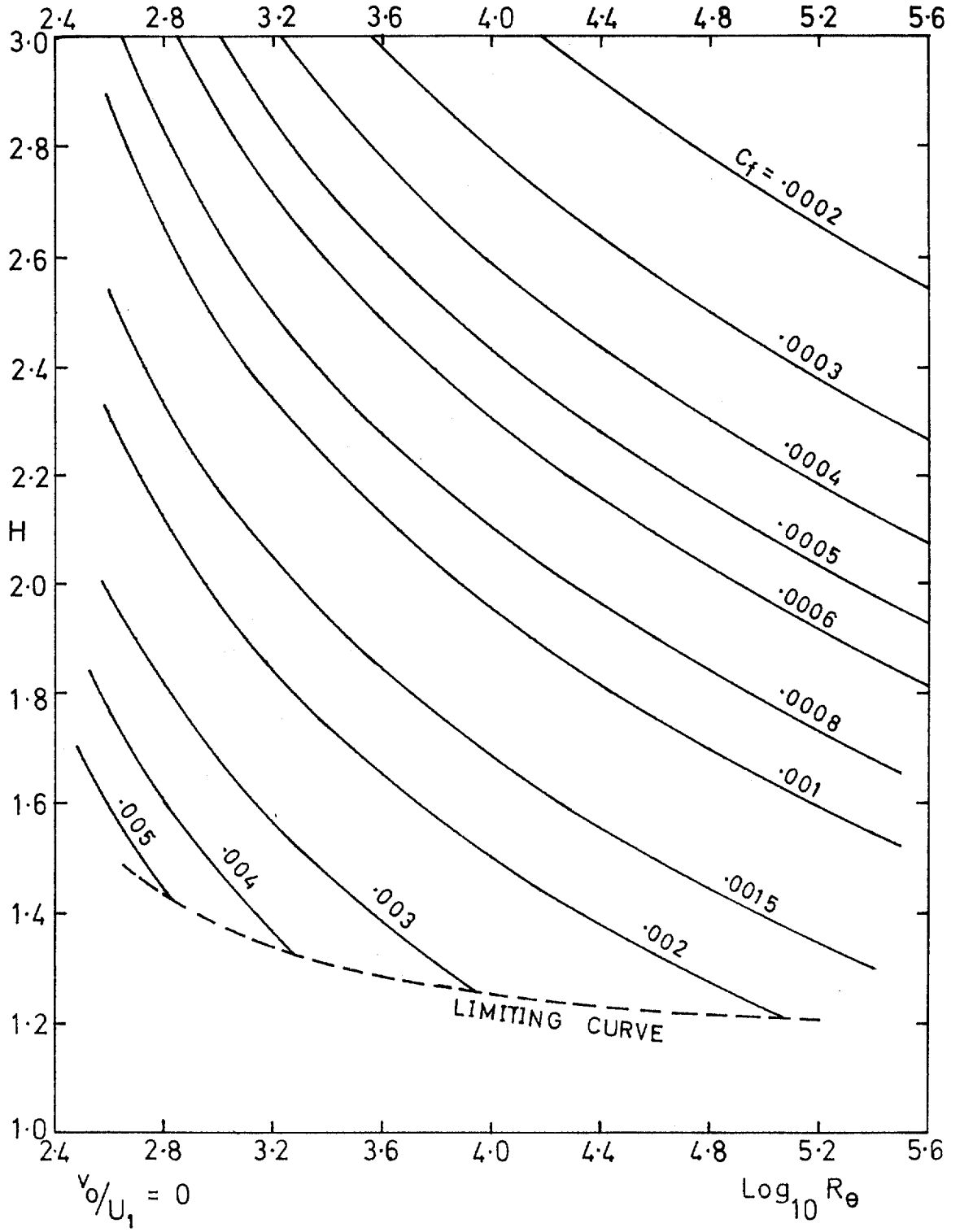

FIG. 8a. The skin-friction law.

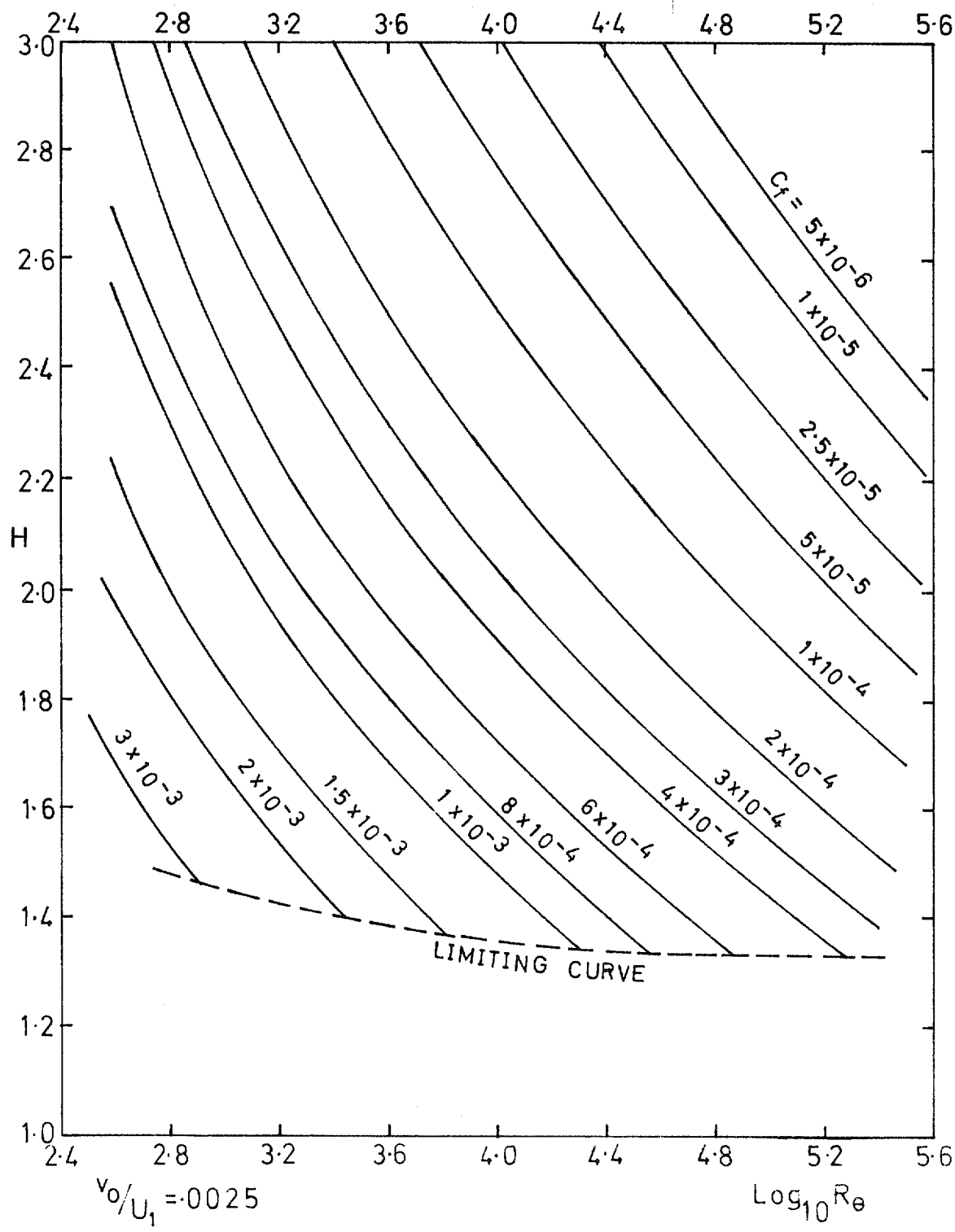

FIG. 8b. The skin-friction law (continued).

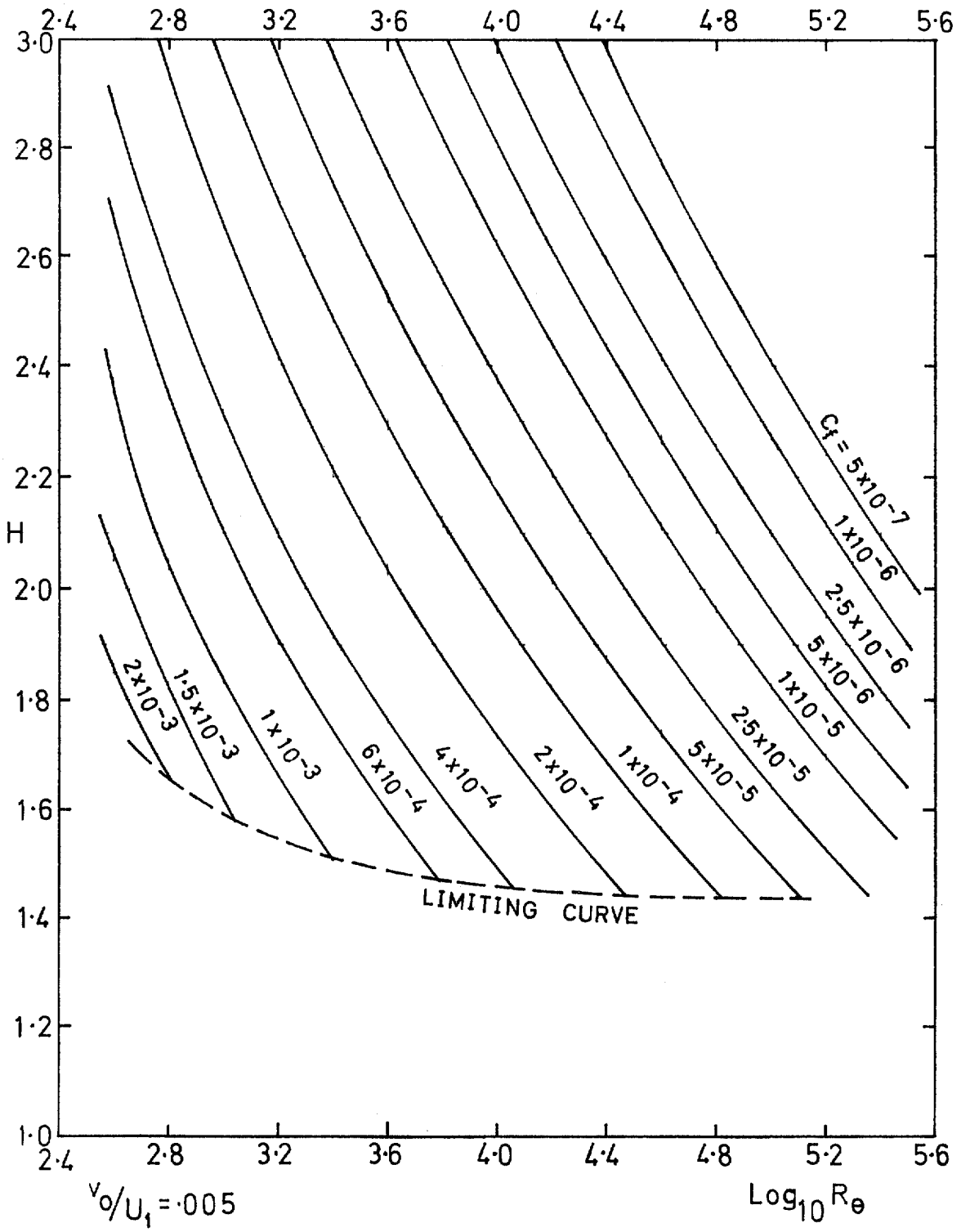

FIG. 8c. The skin-friction law (continued).

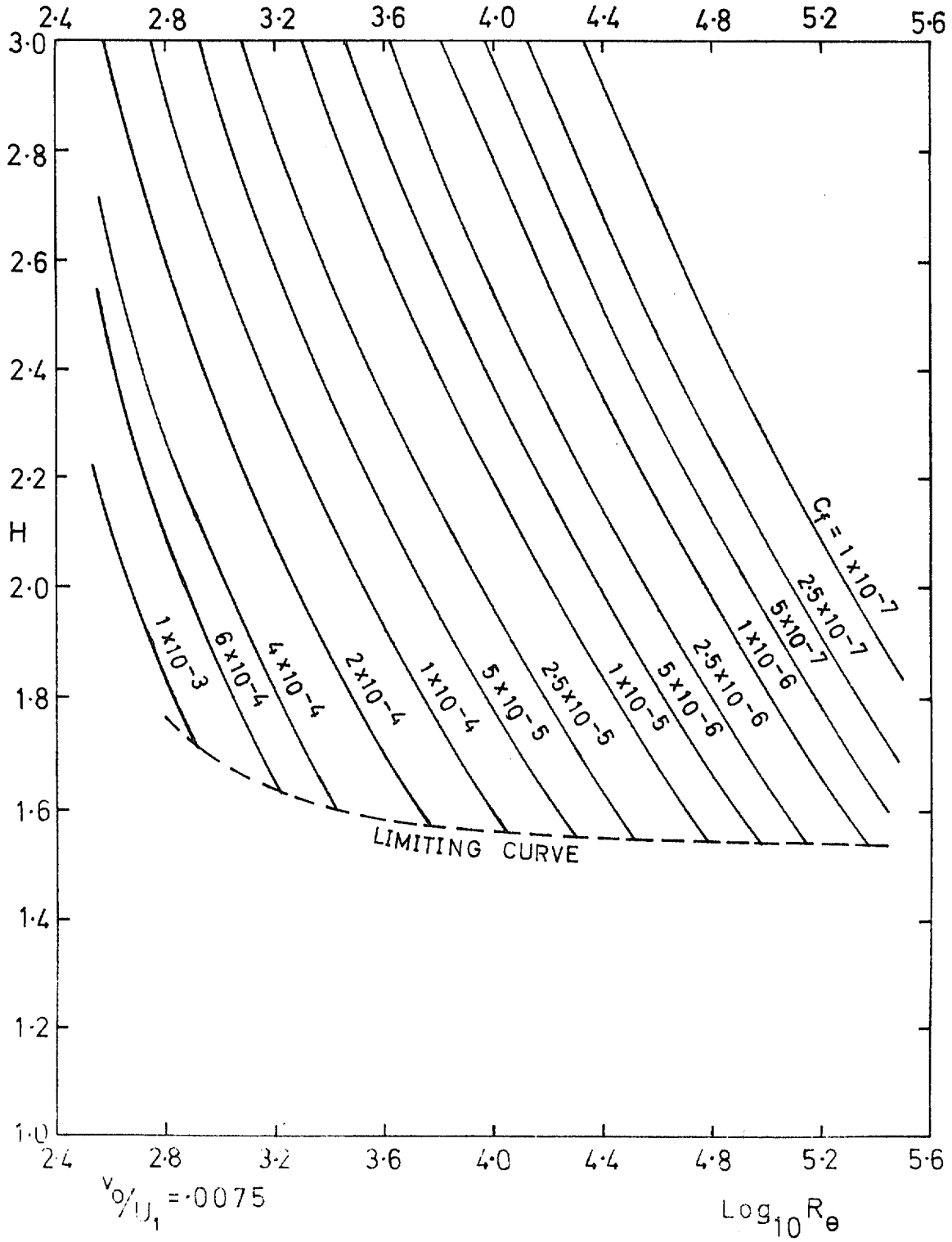

FIG. 8d. The skin-friction law (continued).

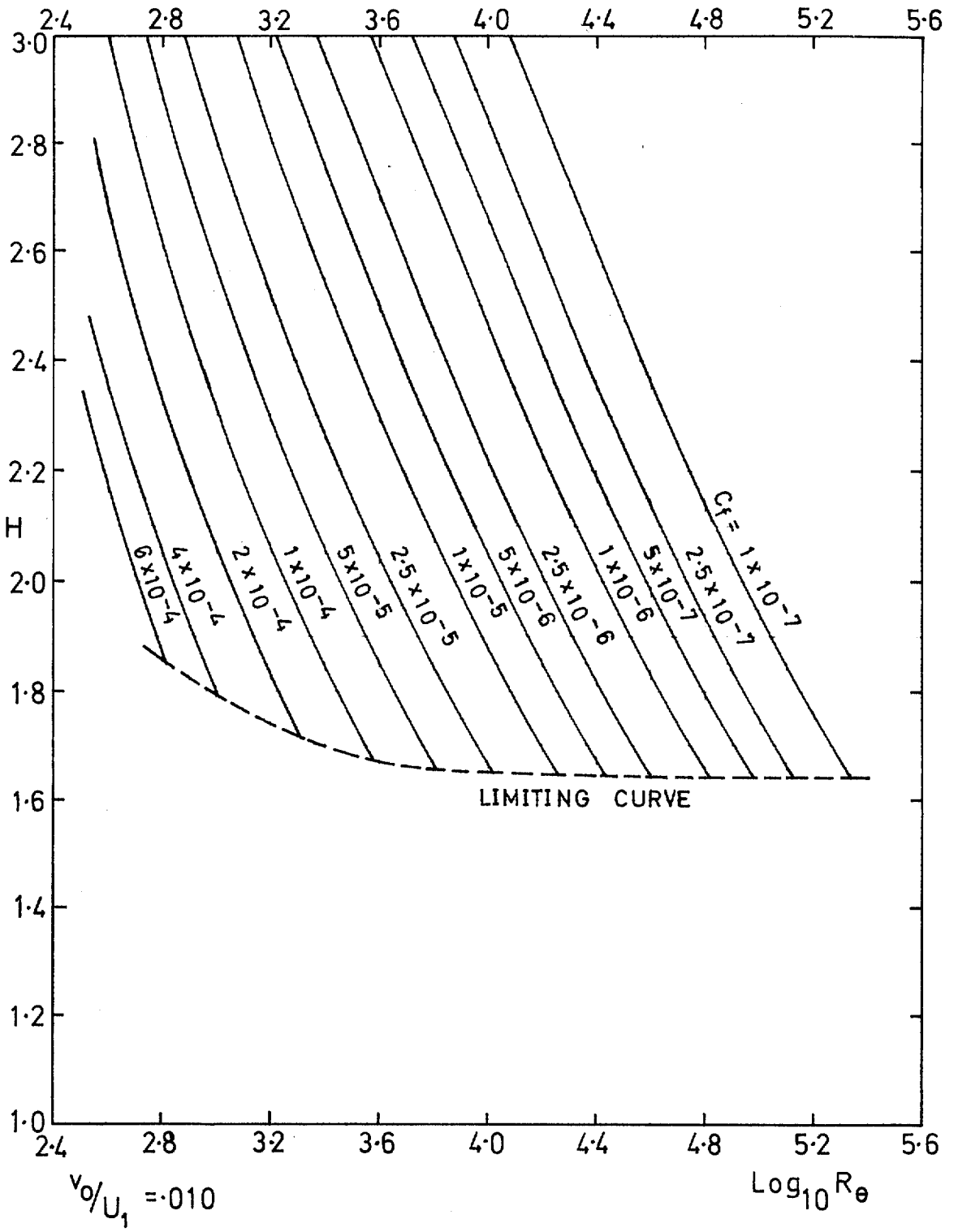

FIG. 8e. The skin-friction law (concluded).

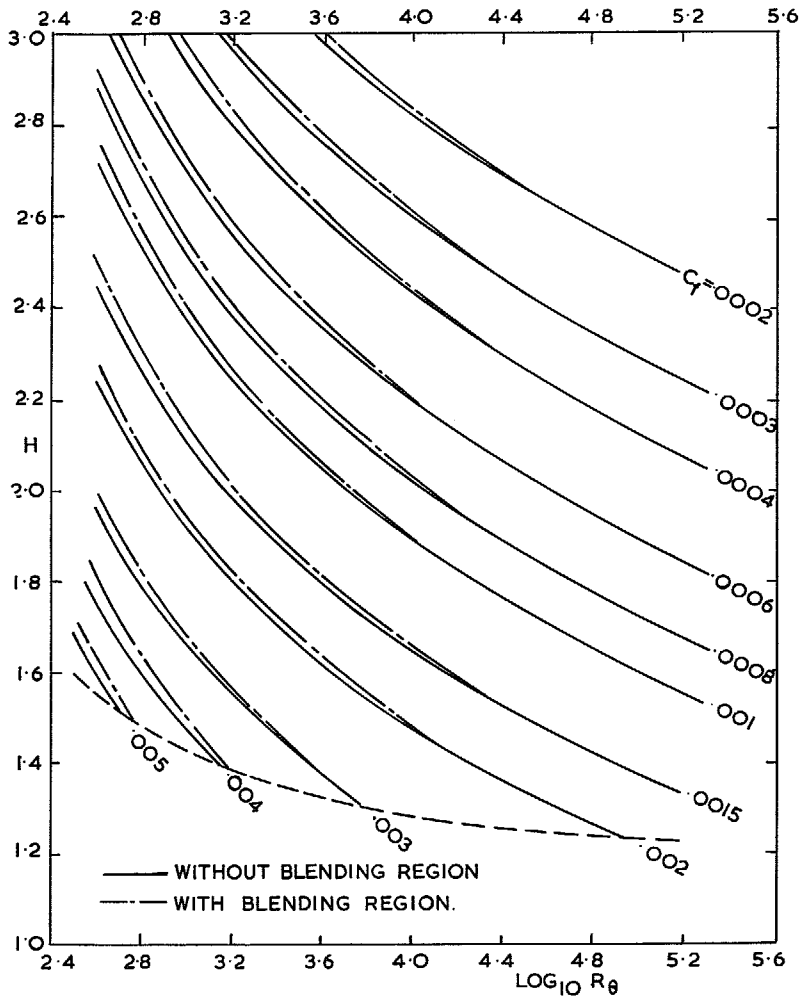

FIG. 9. Effect of sublayer inner-region transition treatment on Thompson's skin-friction law.

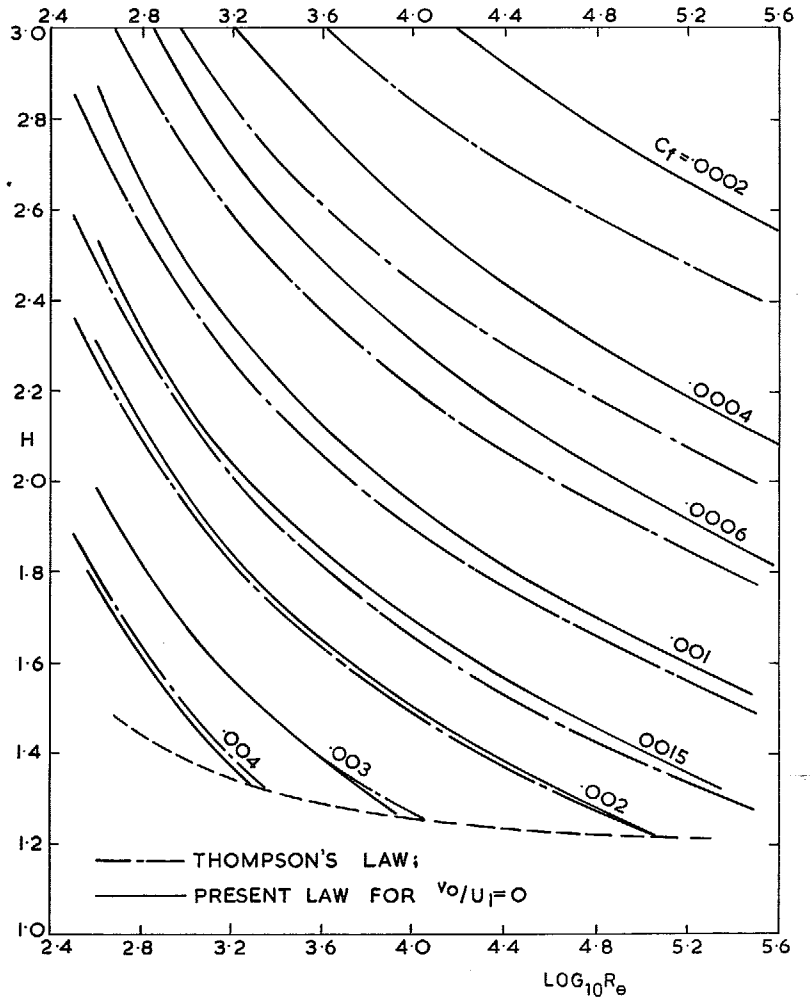

FIG. 10. Comparison of skin-friction laws.

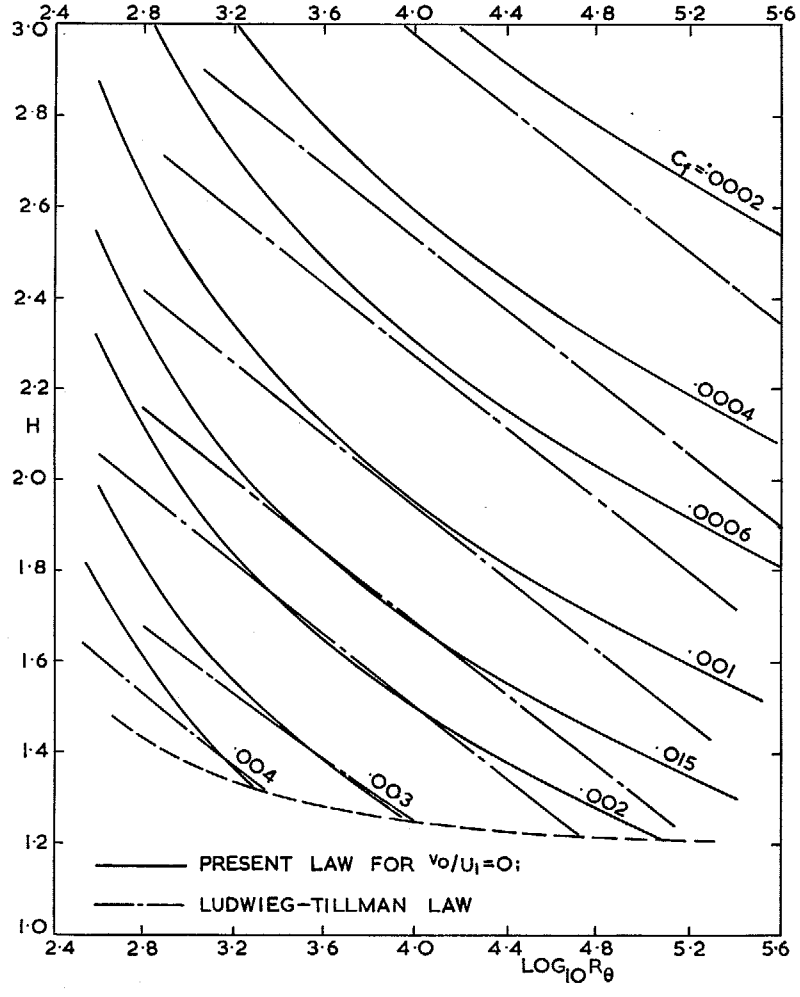

FIG. 11. Comparison of skin-friction laws.

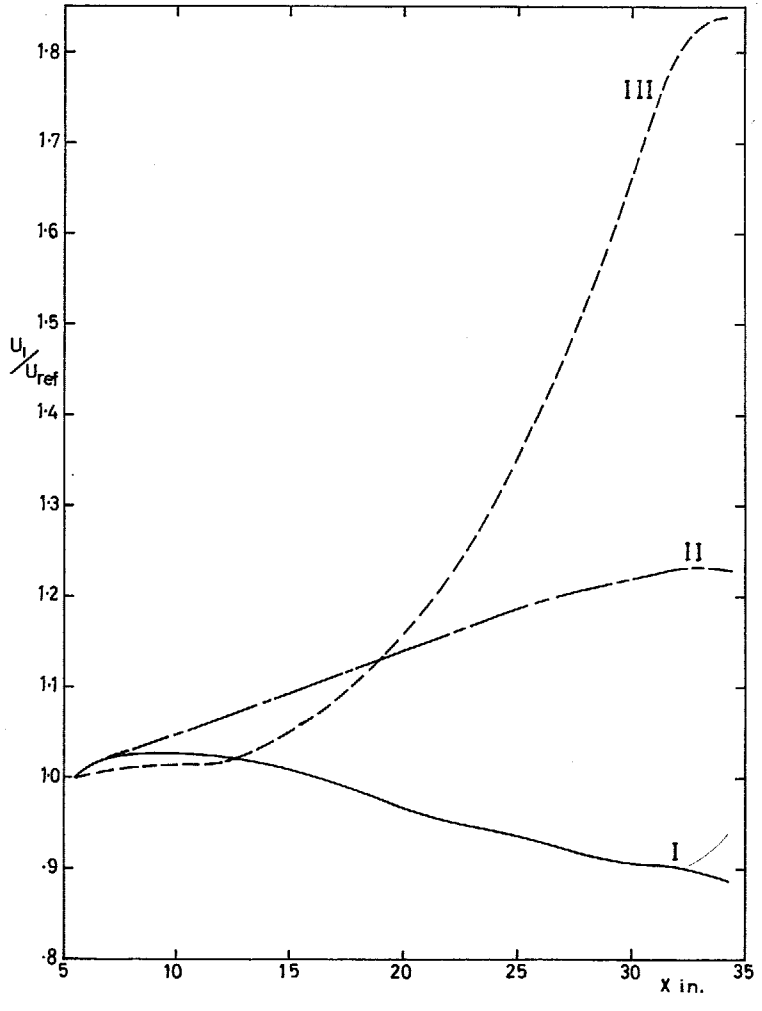

FIG. 12. Distributions of U_1/U_{ref} for layers with pressure gradients.

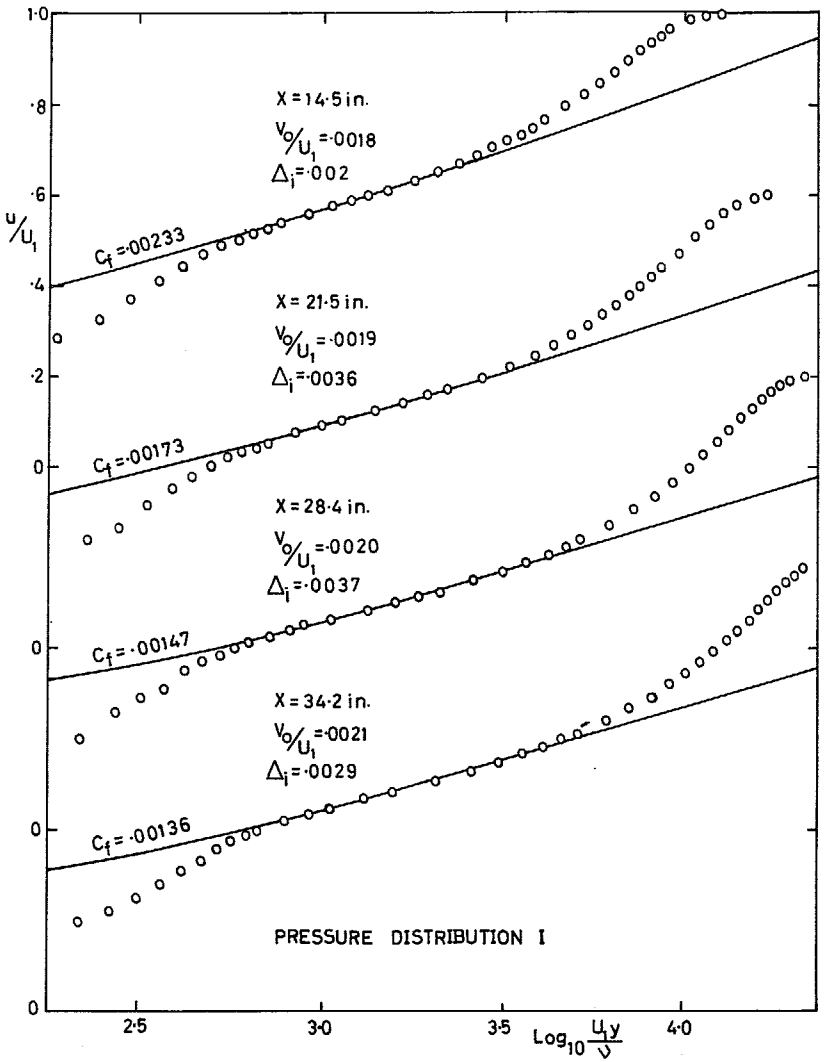

FIG. 13. Comparison of Stevenson's inner-region profile family with experiment.

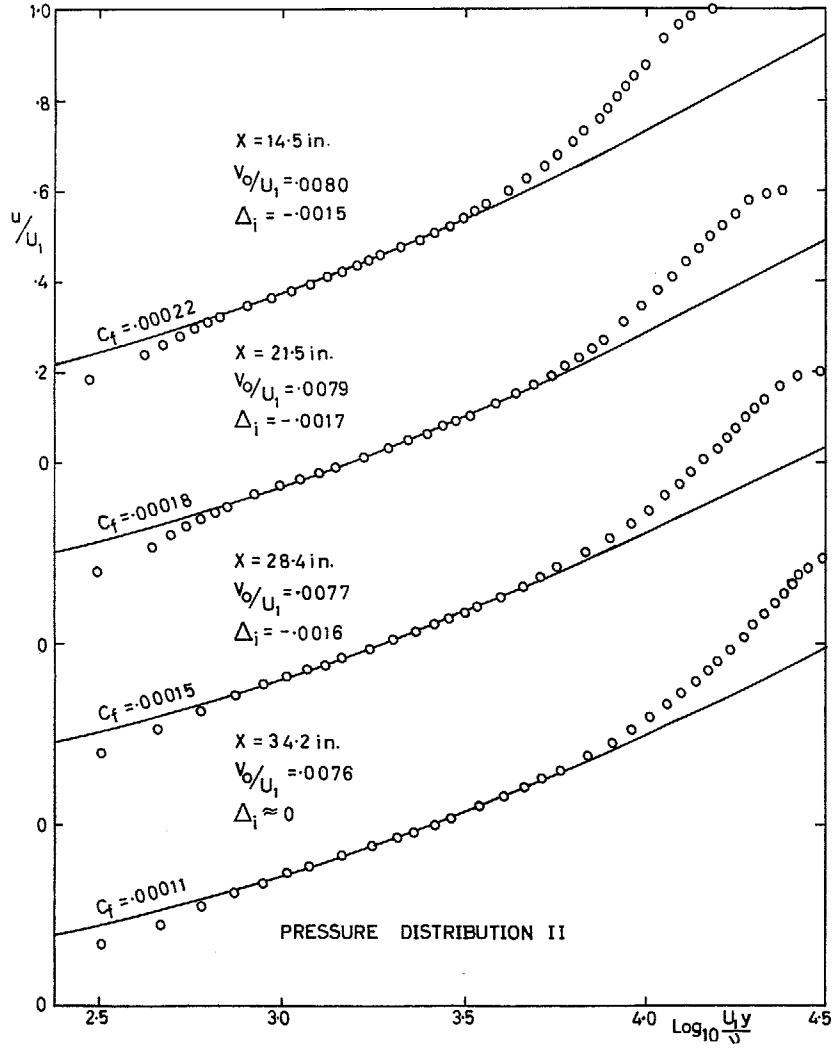

FIG. 14. Comparison of Stevenson's inner-region profile family with experiment.

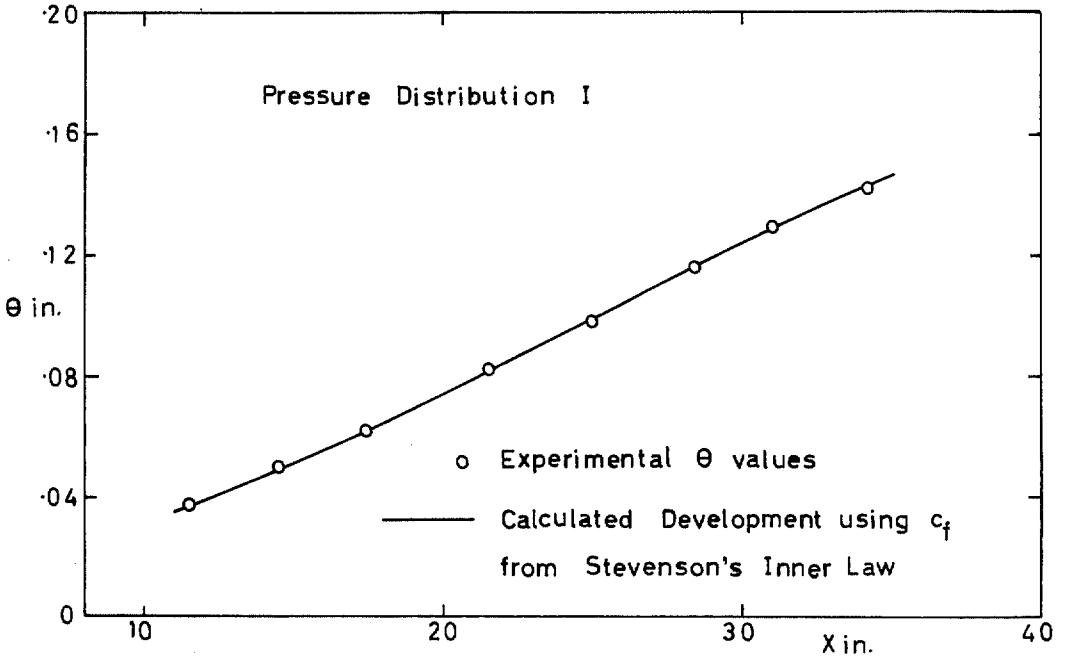

FIG. 15. Comparison of calculated momentum development with experiment.

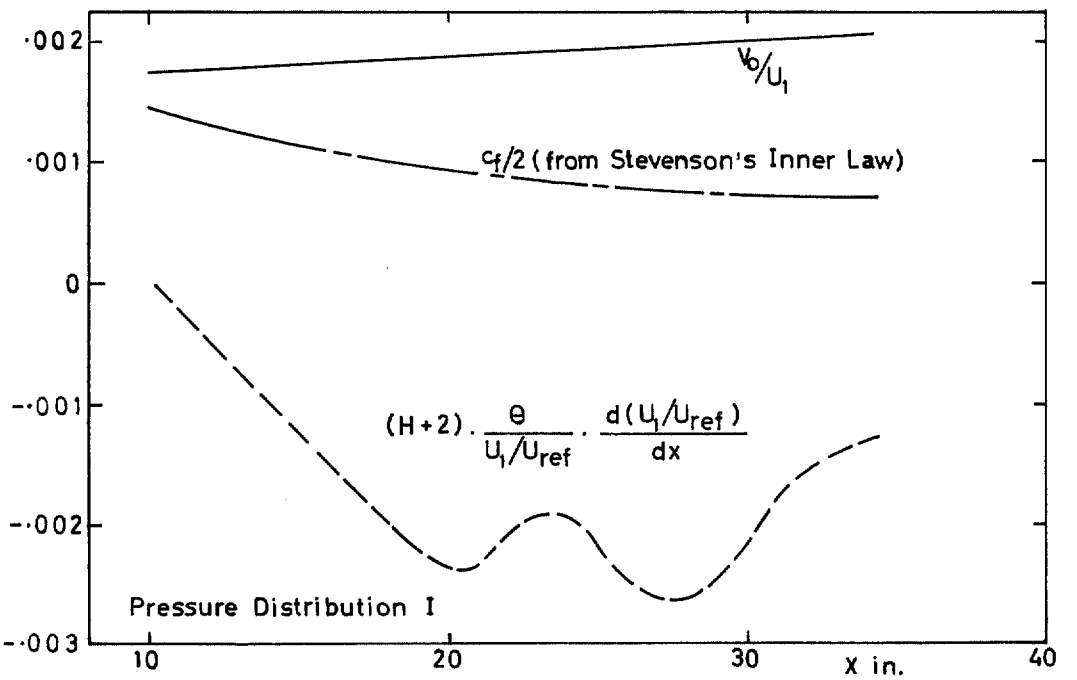

FIG. 16. Distribution of terms in momentum-integral equation.

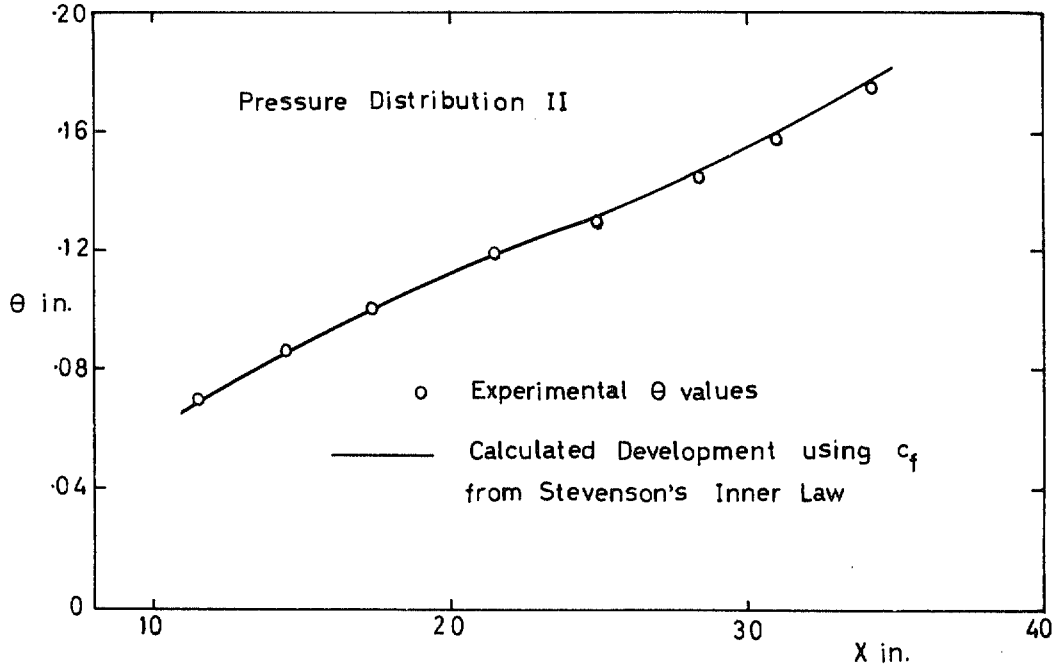

FIG. 17. Comparison of calculated momentum development with experiment.

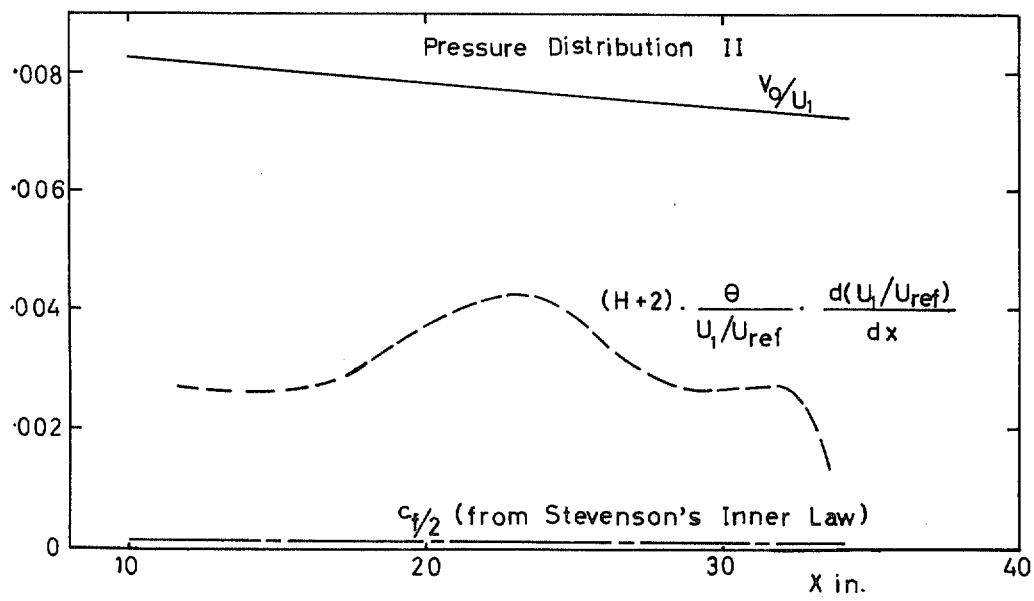

FIG. 18. Distribution of terms in momentum-integral equation.

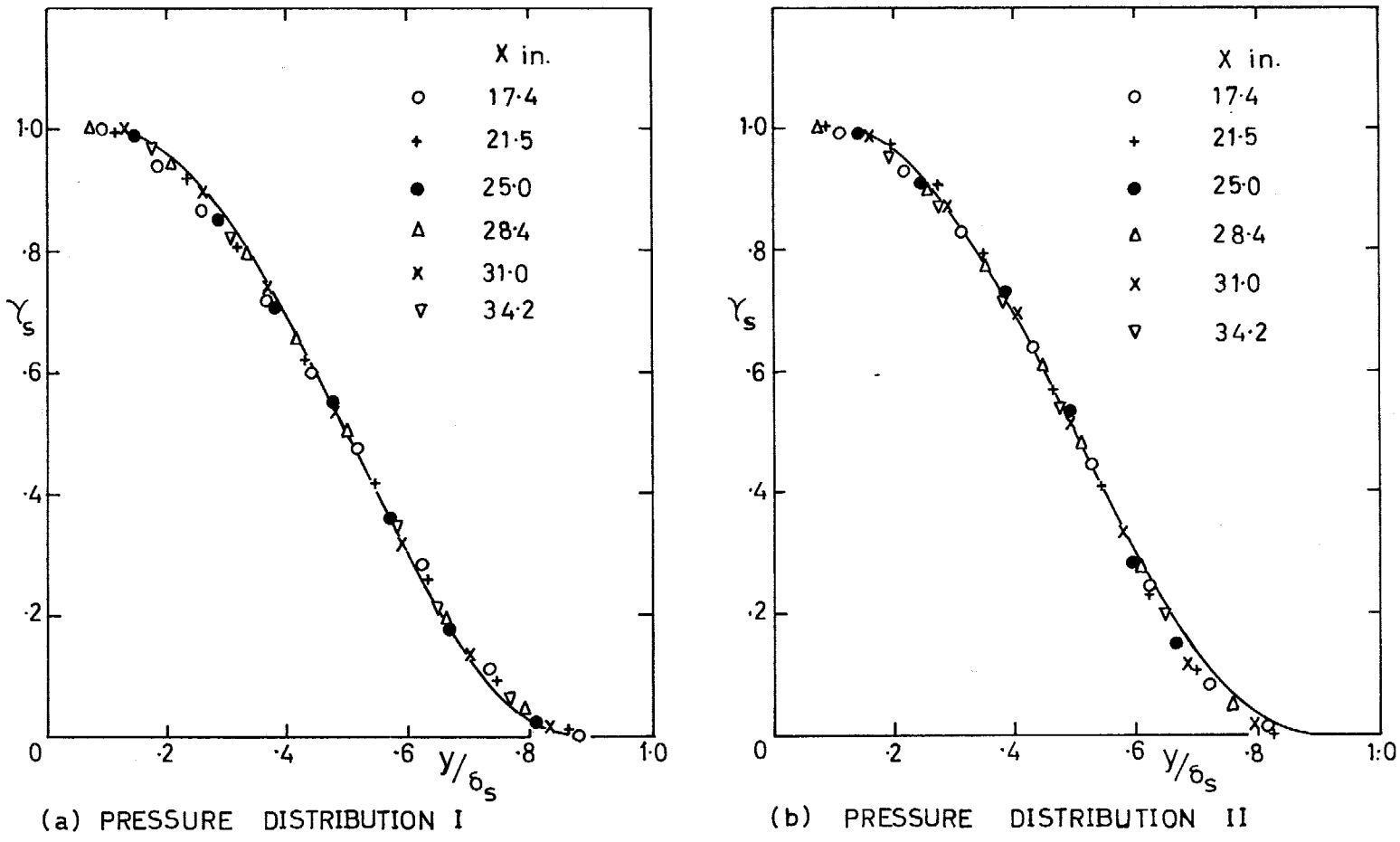

FIG. 19. Comparison of intermittency distributions with zero pressure-gradient mean curve.

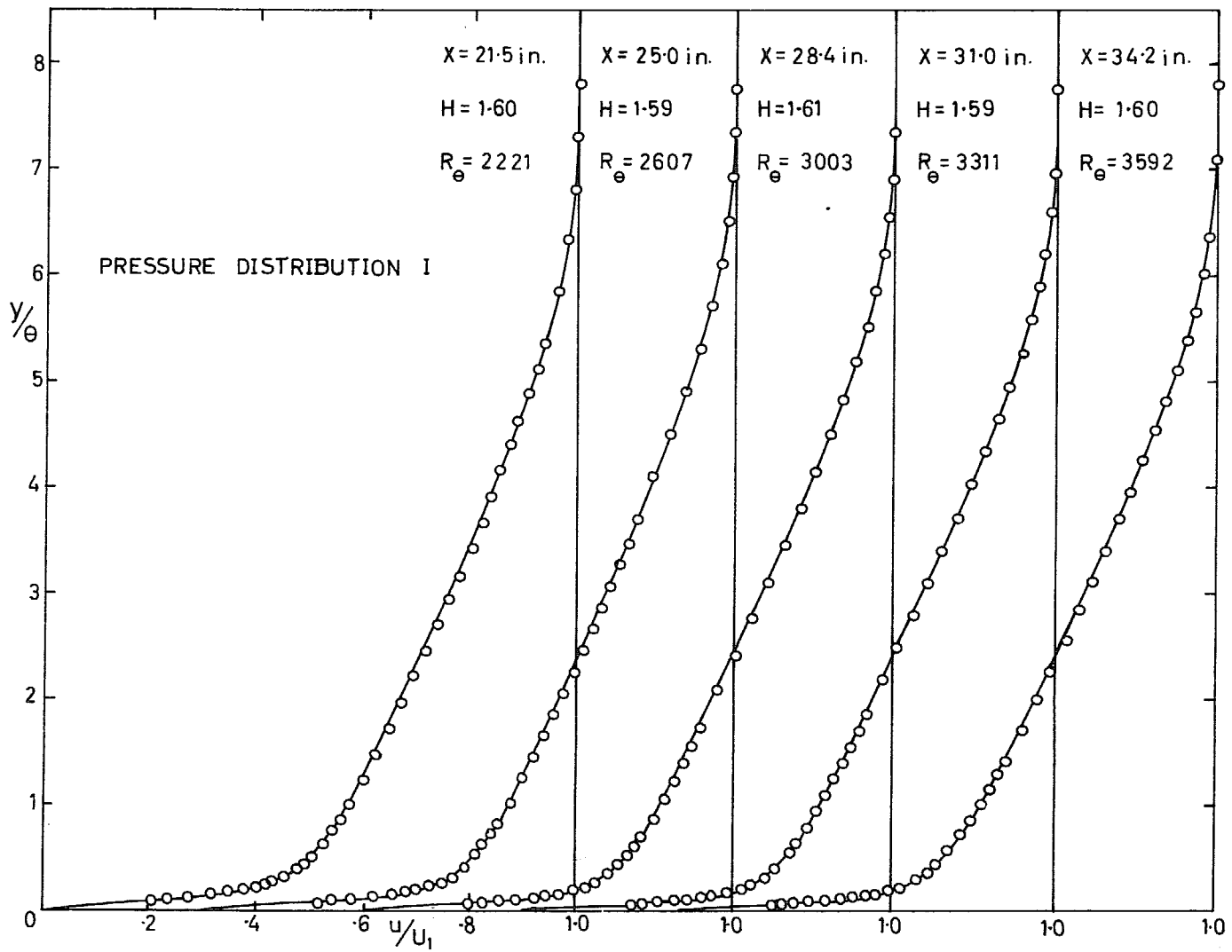

FIG. 20. Comparison of the profile family with experiment.

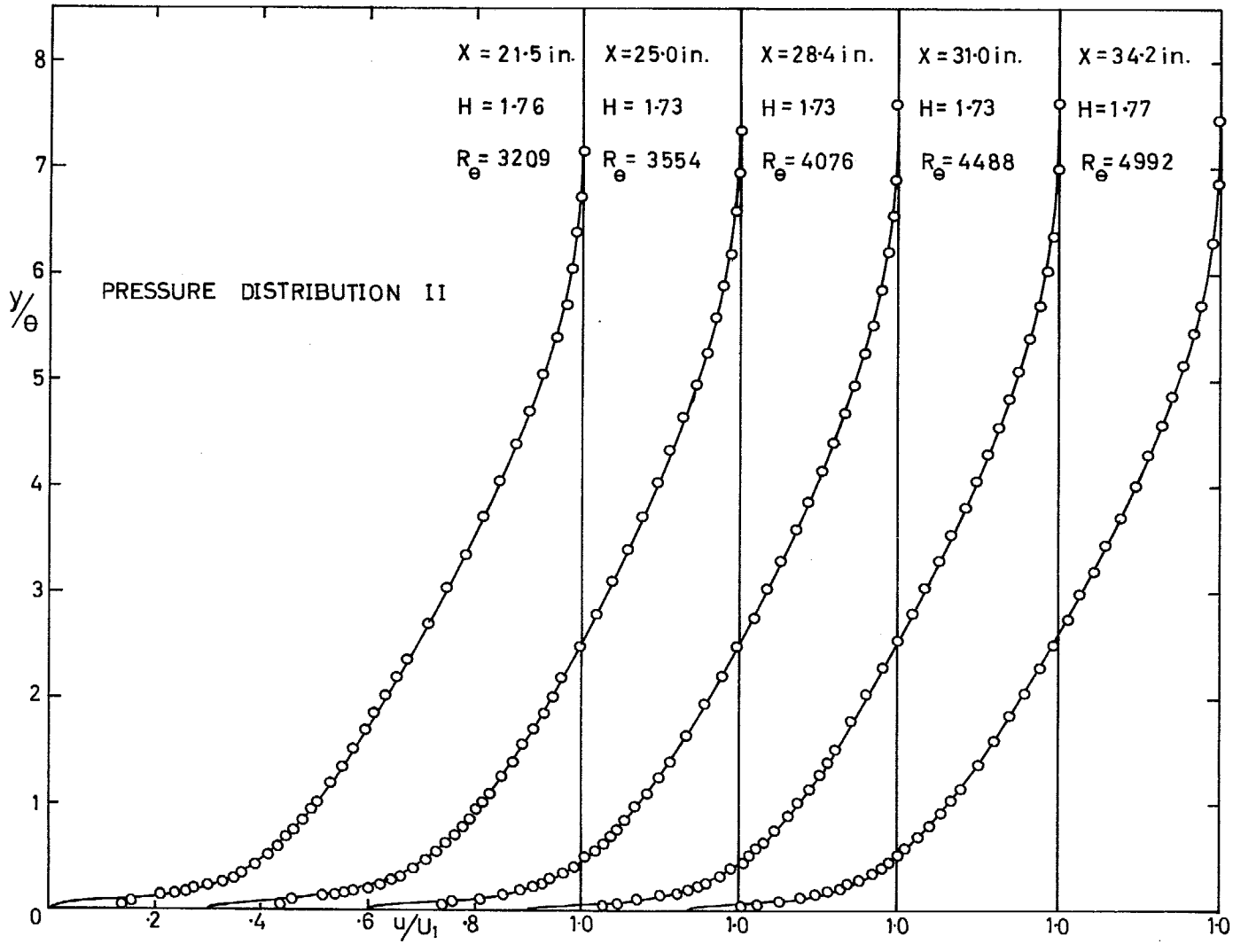

FIG. 21. Comparison of the profile family with experiment.

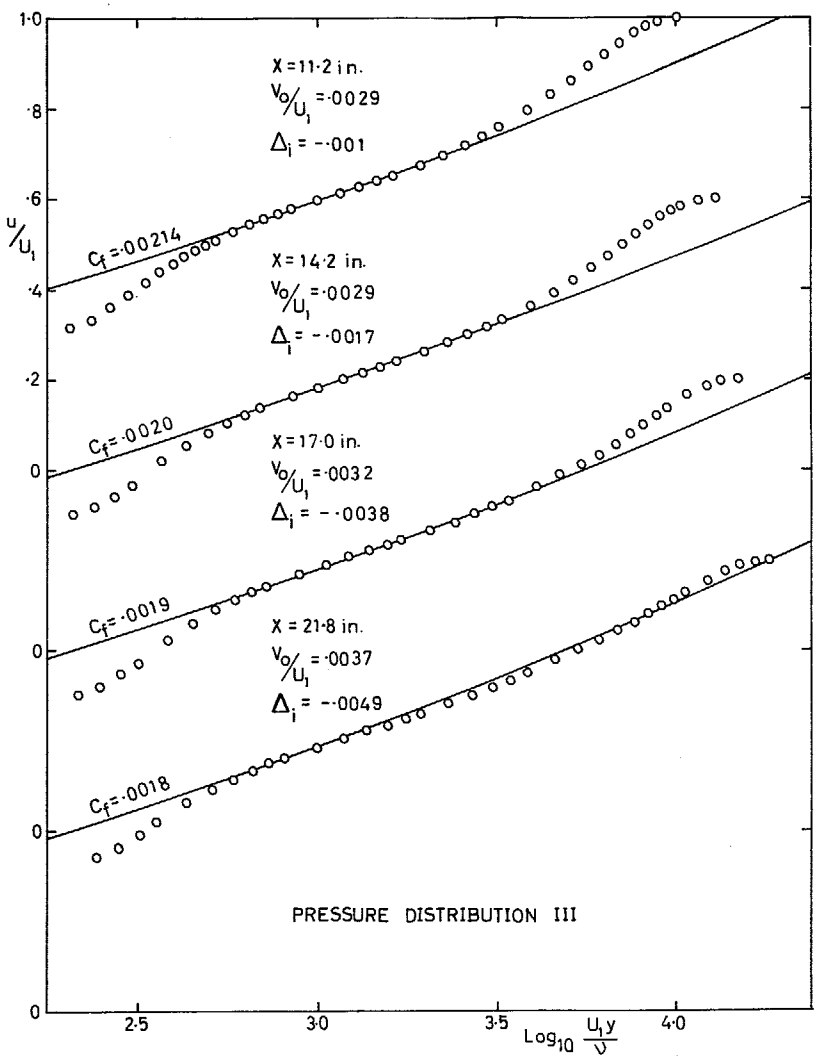

FIG. 22a. Comparison of Stevenson's inner-region profile family with experiment.

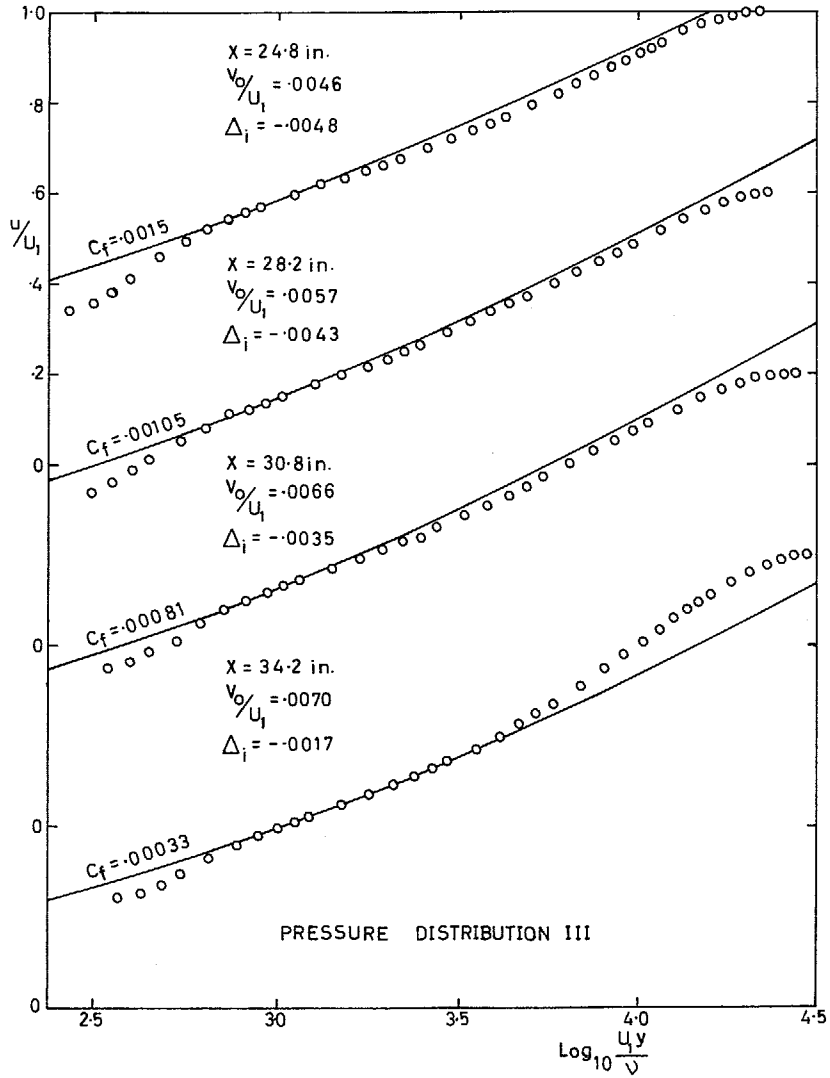

FIG. 22b. Comparison of Stevenson's inner-region profile family with experiment.

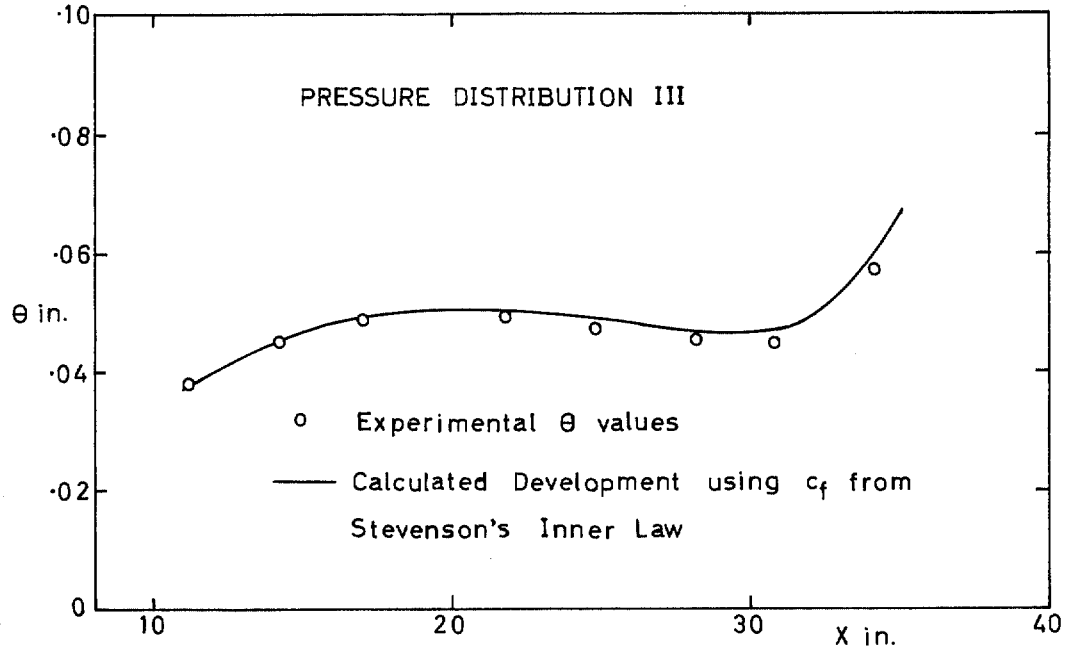

FIG. 23. Comparison of calculated momentum development with experiment.

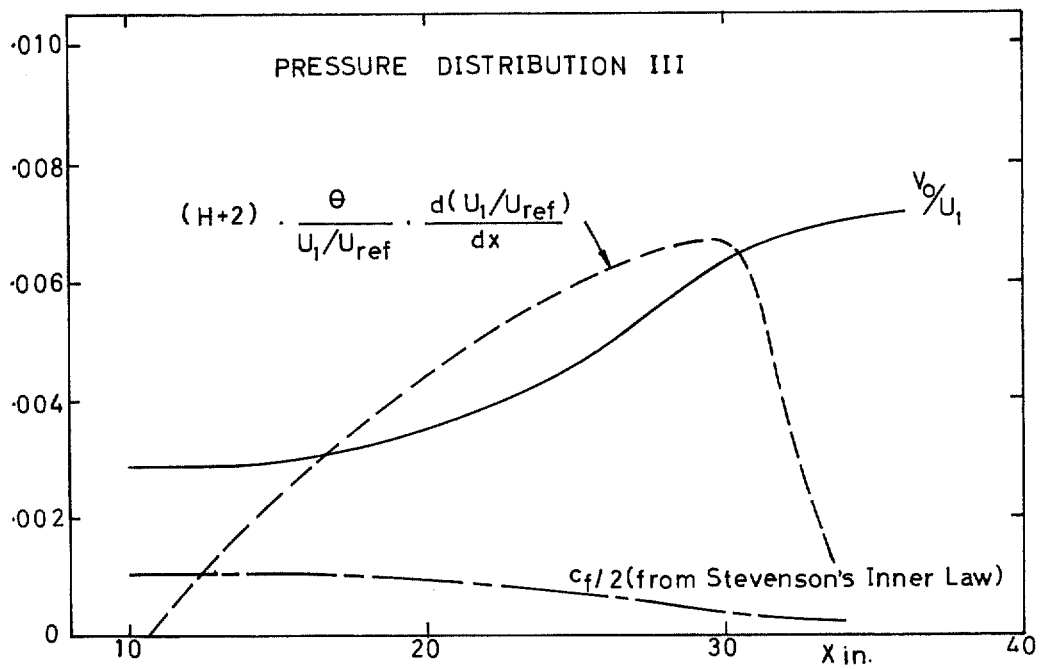

FIG. 24. Distribution of terms in momentum-integral equation.

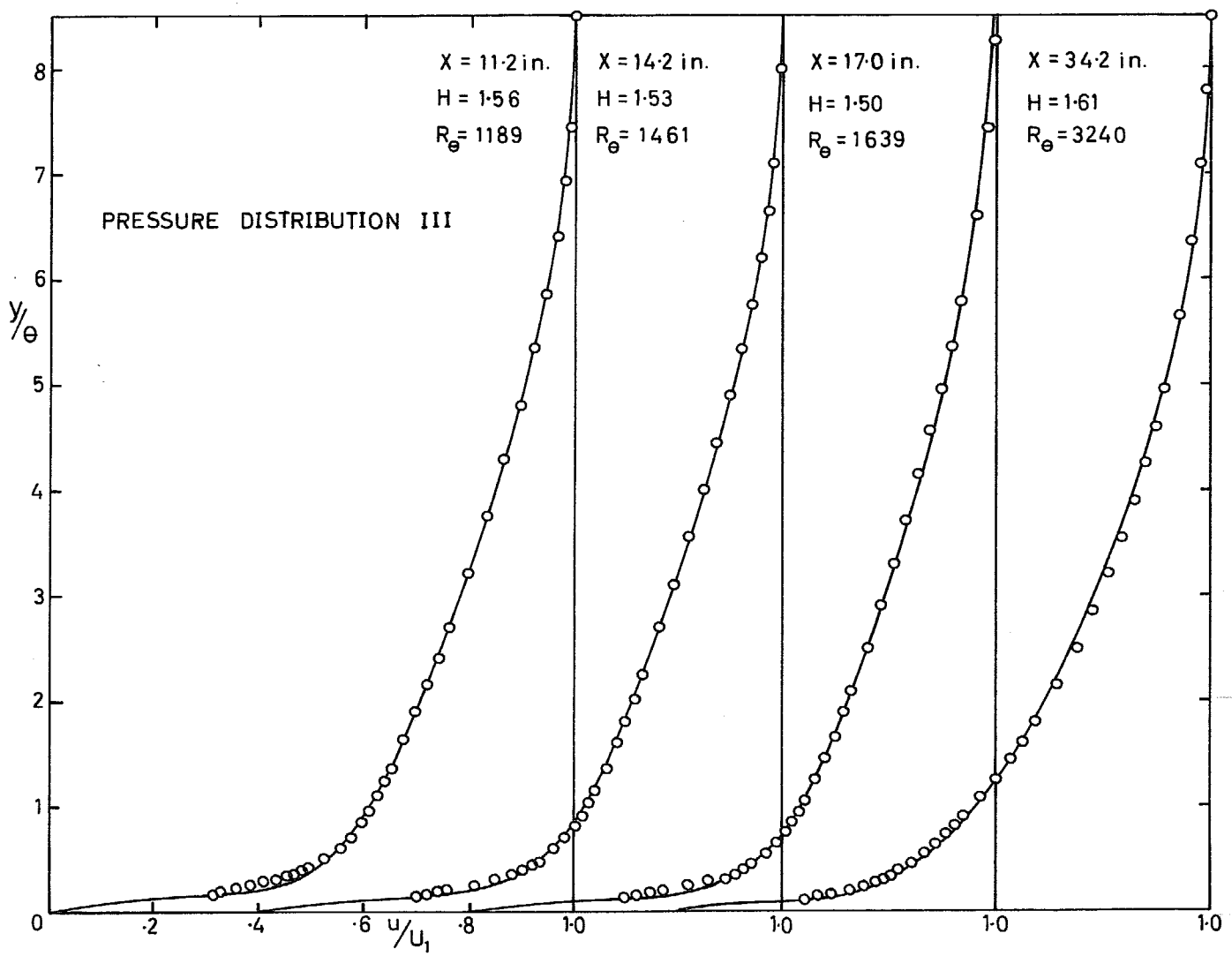

FIG. 25. Comparison of the profile family with experiment.

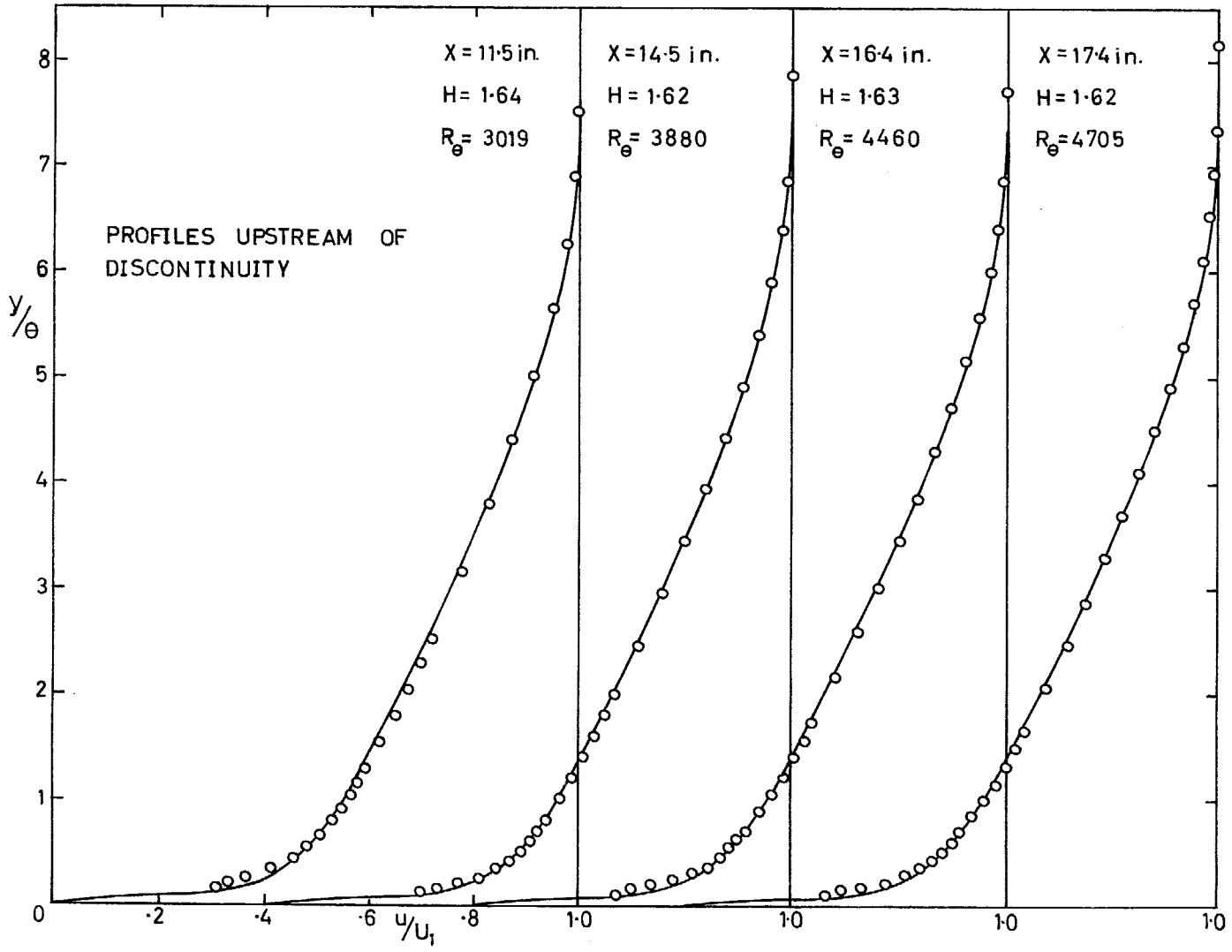

FIG. 26. Comparison of the profile family with experiment.

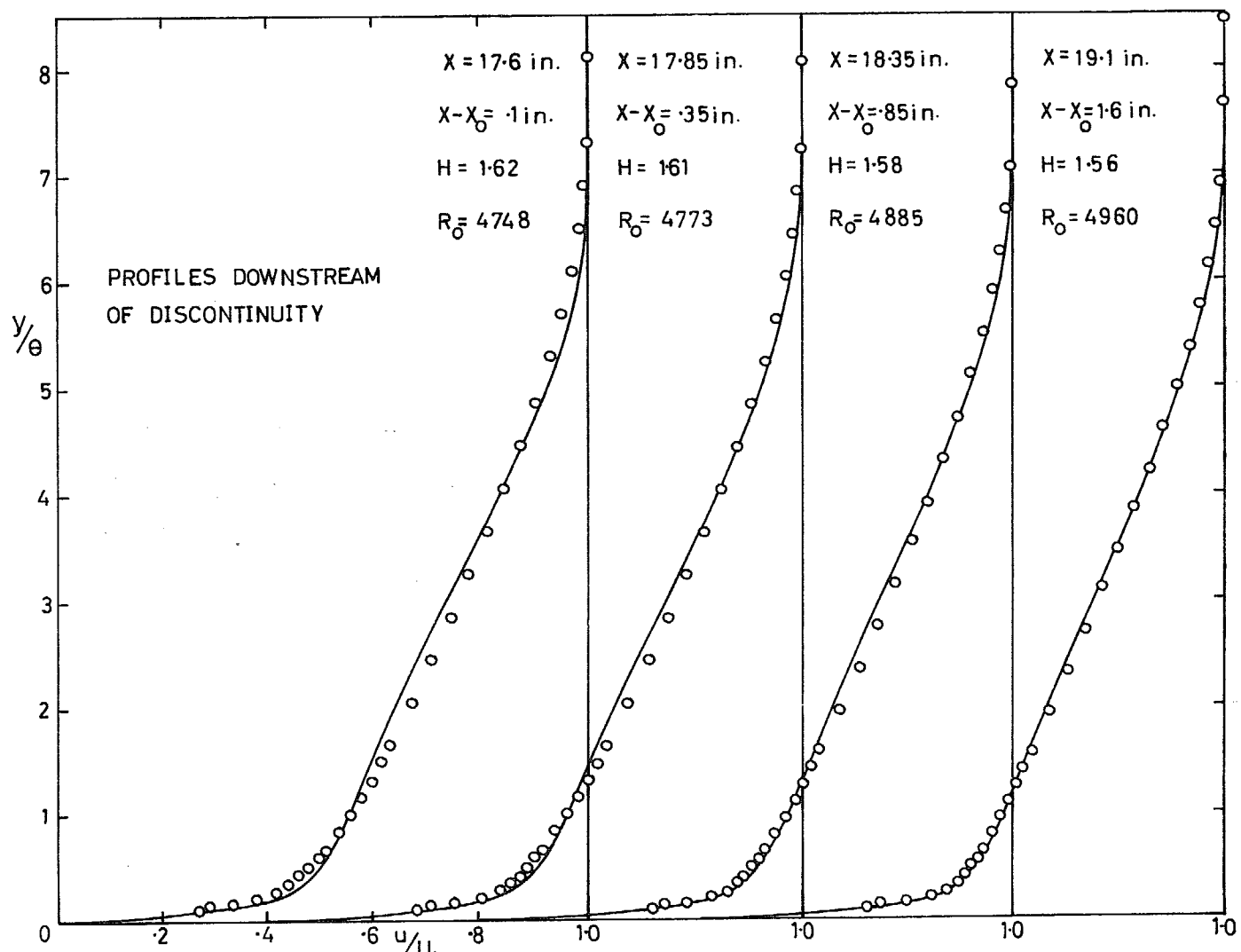

FIG. 27a. Comparison of the profile family with experiment.

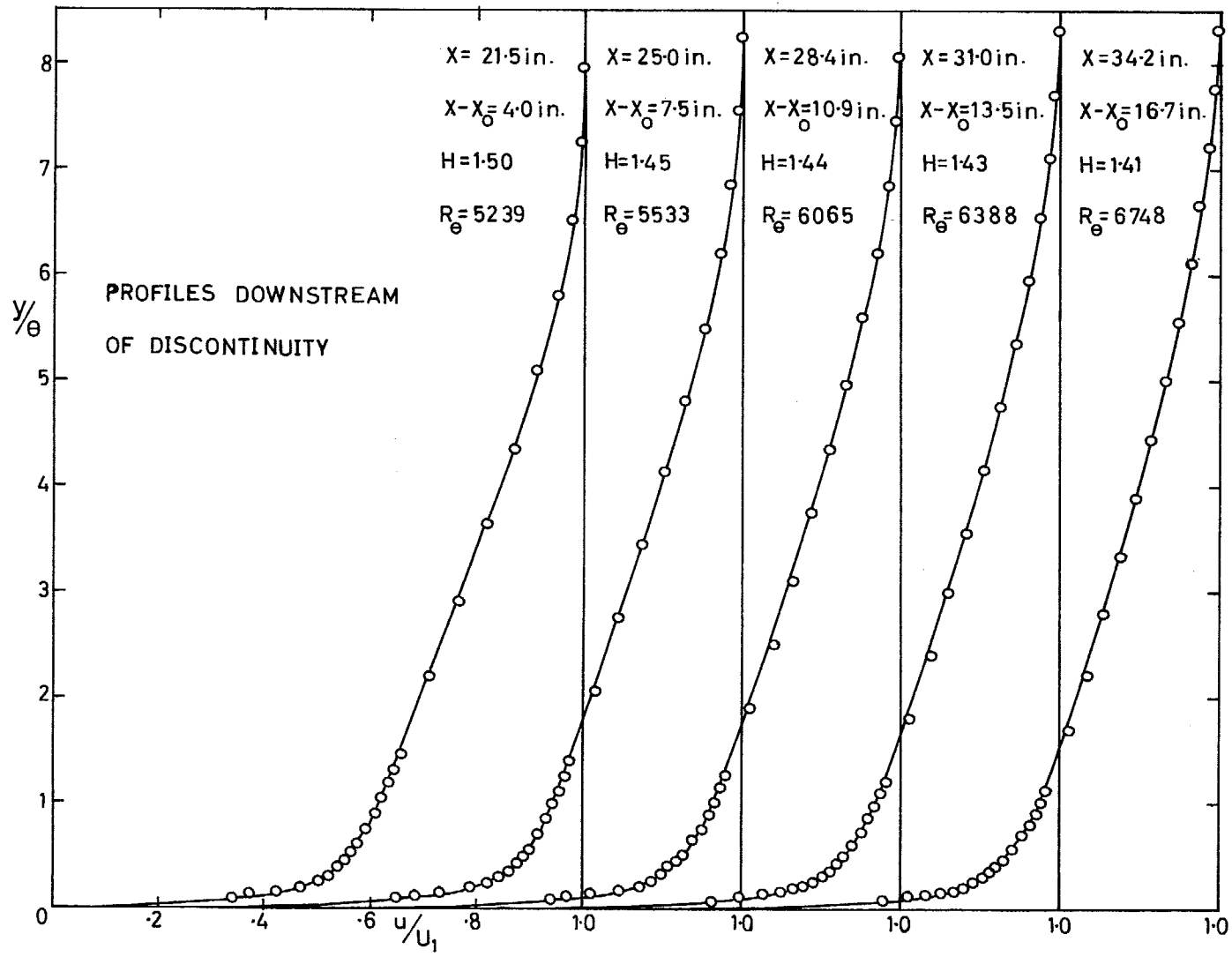

FIG. 27b. (concl.). Comparison of the profile family with experiment.

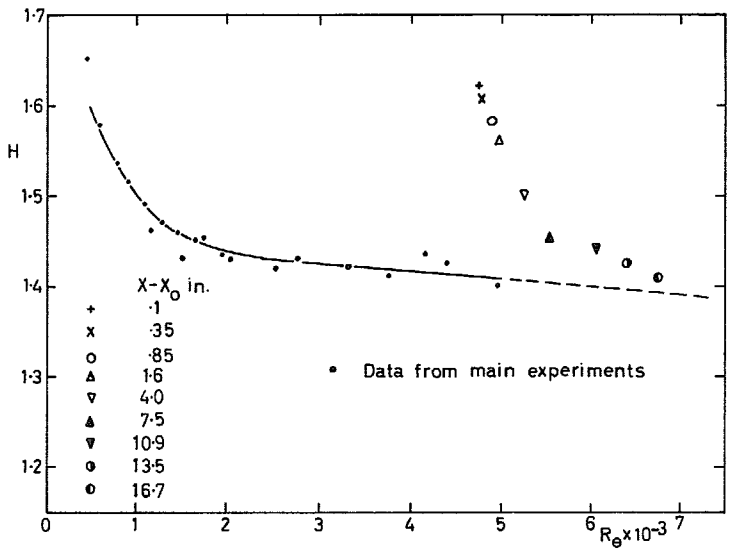

FIG. 28. Comparison of H with curve for fully developed conditions.

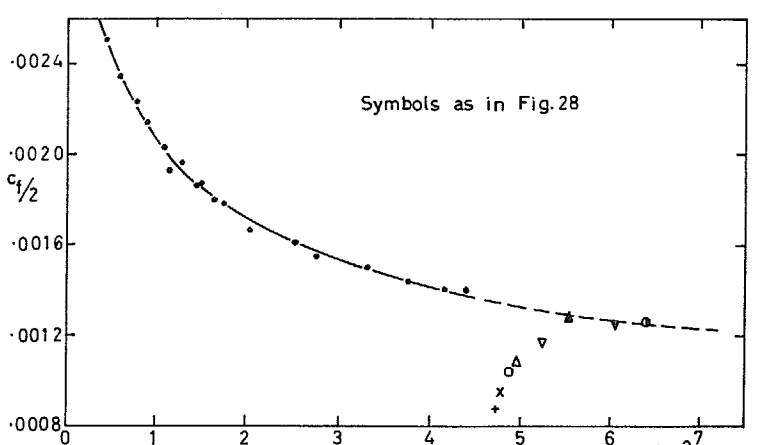

FIG. 29. Comparison of Preston tube c_f with curve for fully developed conditions.

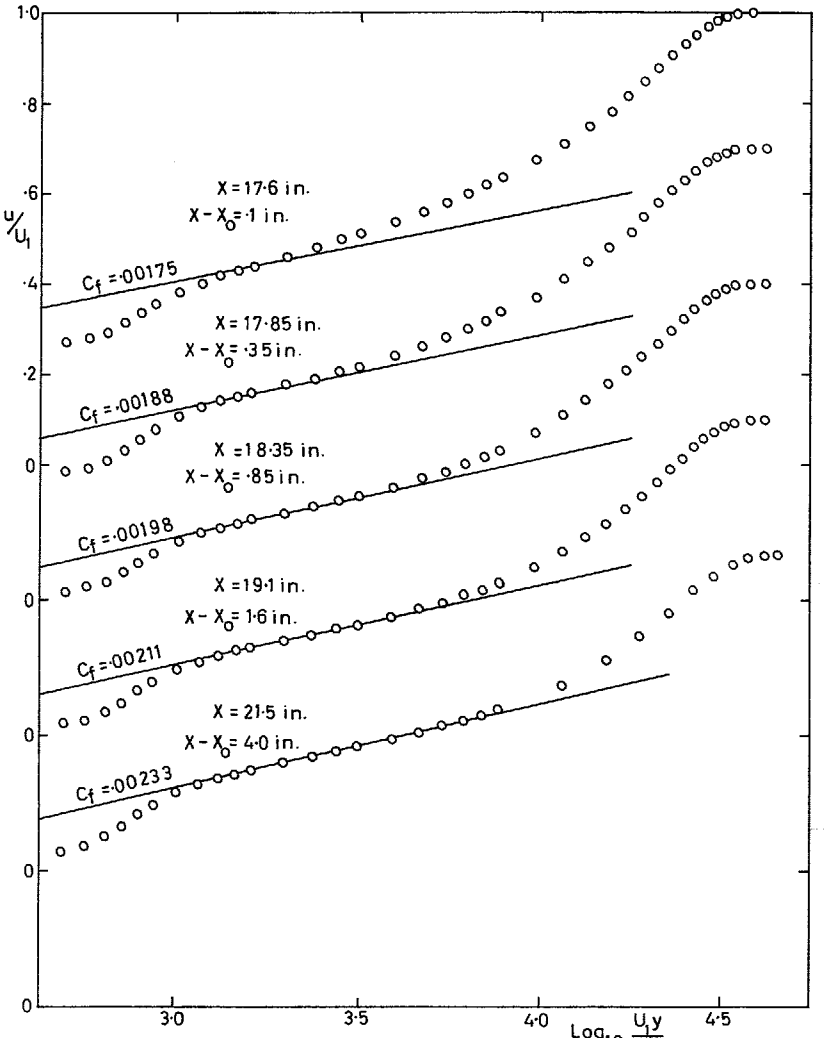

FIG. 30. Comparison of profiles downstream of discontinuity with semi-log law (Clauser plot).

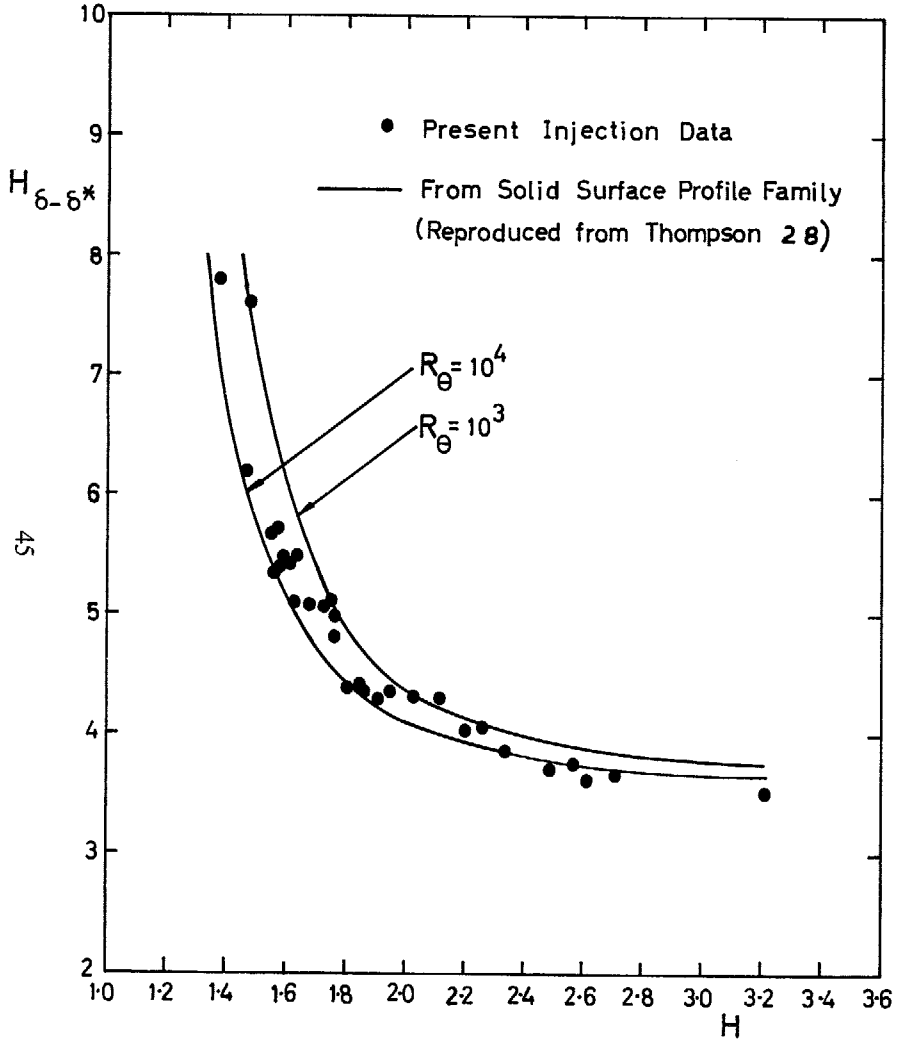

FIG. 31. Comparison of injection data with solid surface shape-factor relationship.

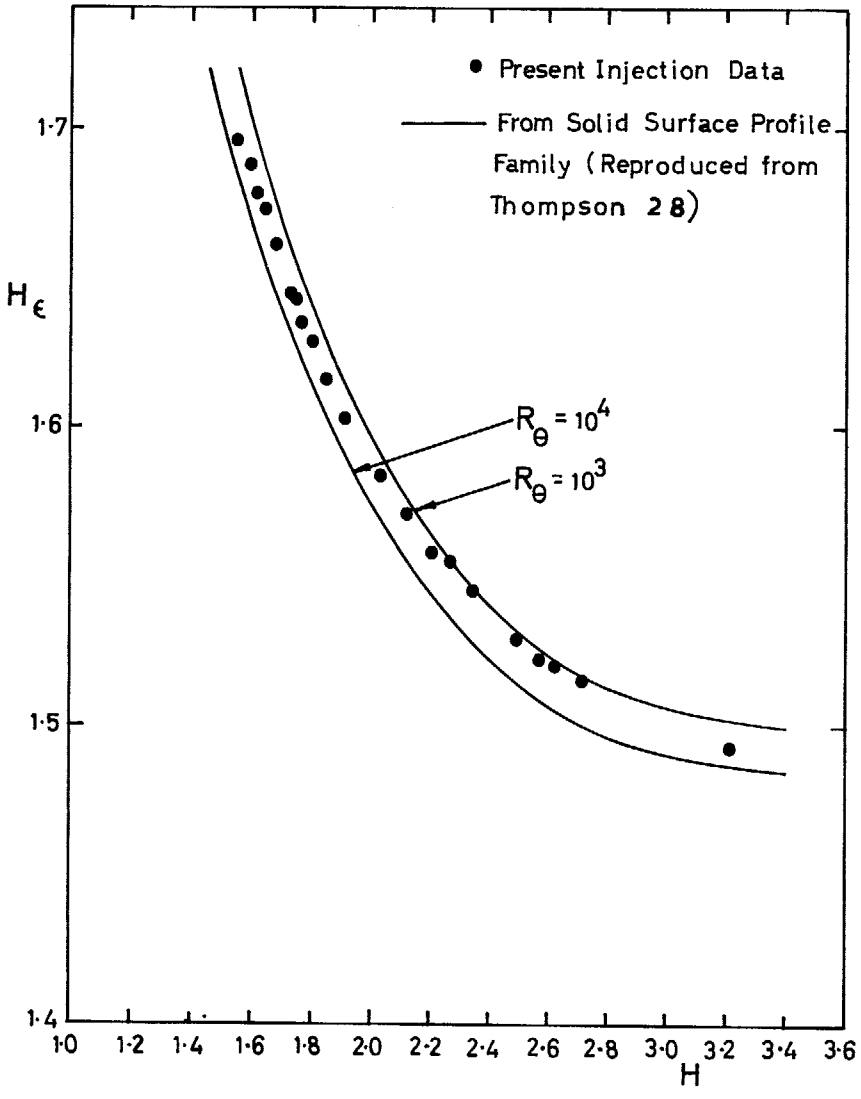

FIG. 32. Comparison of injection data with solid-surface shape-factor relationship.

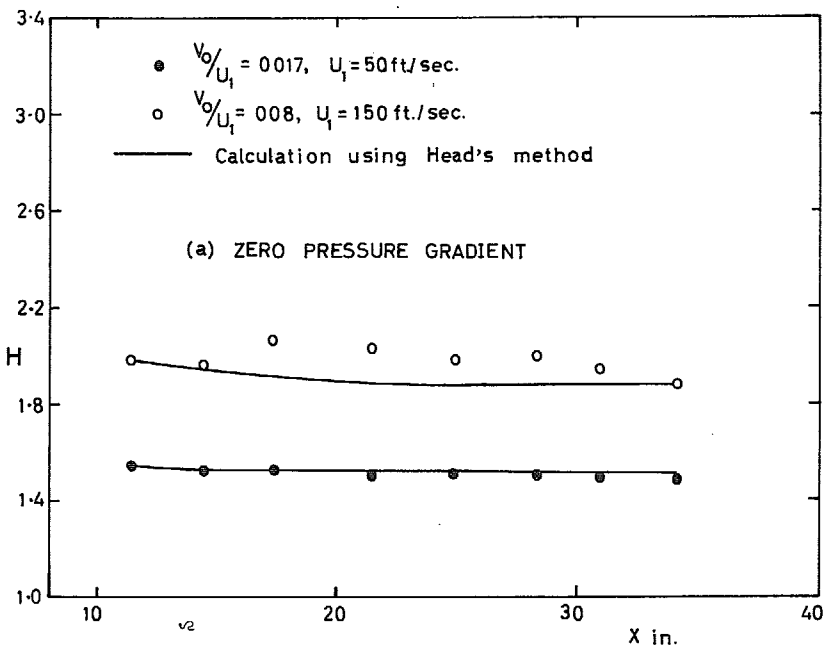

FIG. 33. Comparison of shape-factor calculations with experiment.

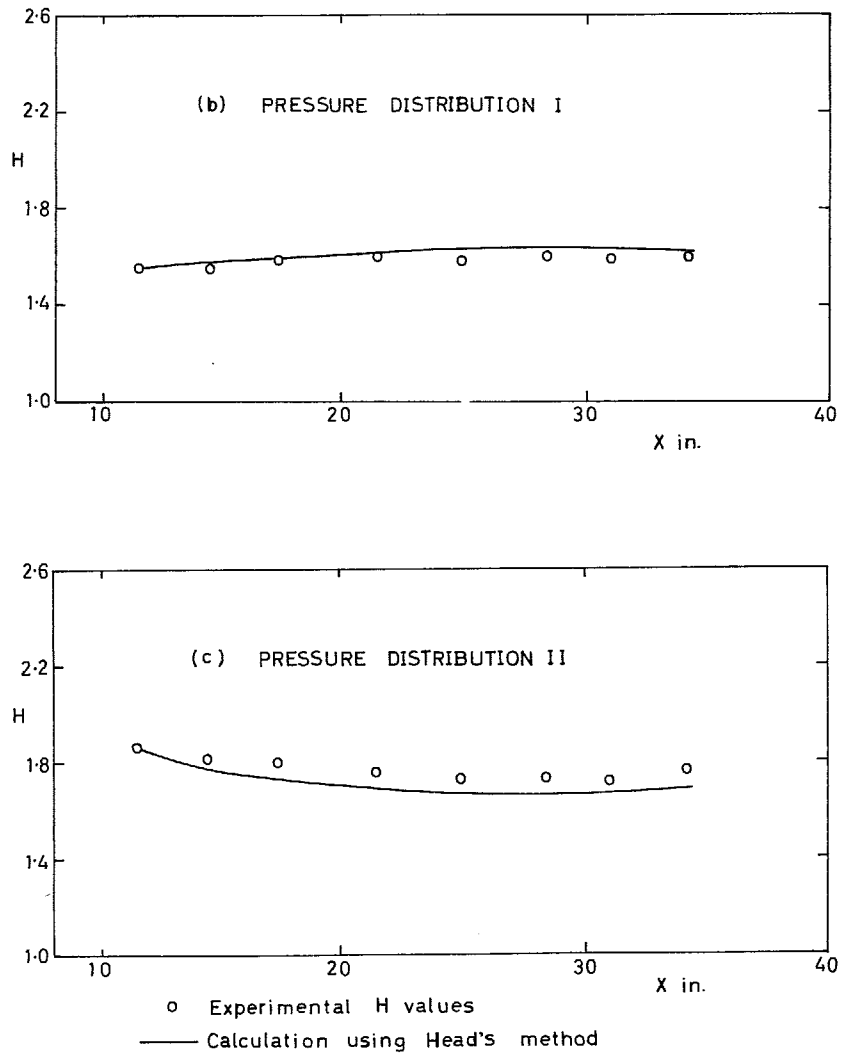

FIG. 33. (contd.). Comparison of shape-factor calculations with experiment.

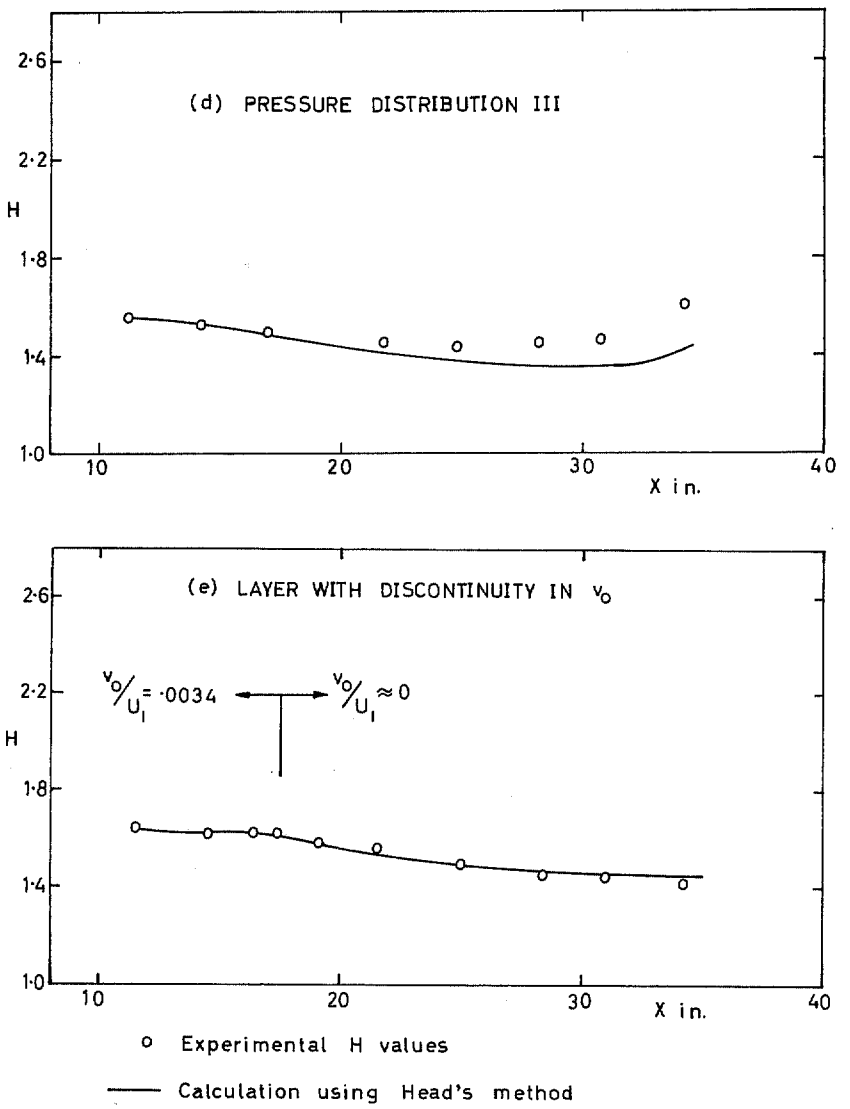

FIG. 33. (concl.). Comparison of shape-factor calculations with experiment.

Printed in Wales for Her Majesty's Stationery Office by Allens Printers (Wales) Limited

Dd.129527 K.5

Published by
HER MAJESTY'S STATIONERY OFFICE

To be purchased from
49 High Holborn, London W.C.1
423 Oxford Street, London W.1
13A Castle Street, Edinburgh 2
109 St. Mary Street, Cardiff CF1 1JW
Brazennose Street, Manchester 2
50 Fairfax Street, Bristol 1
258–259 Broad Street, Birmingham 1
7–11 Linenhall Street, Belfast BT2 8AY
or through any bookseller